Styrene Oxide Adducts in an Oligodeoxynucleotide Containing the Human *N-ras* Codon 12 Sequence: Structural Refinement of the Minor Groove R(12,2)- and S(12,2)-α-(*N*^{2}-Guanyl) Stereoisomers from ^{1}H NMR†

Irene S. Zegar, Feloora R. Setayesh, Bart L. DeCorte,‡ Constance M. Harris, Thomas M. Harris, and Michael P. Stone*

Center for Molecular Toxicology and Department of Chemistry, Vanderbilt University, Nashville, Tennessee 37235

Received September 1, 1995; Revised Manuscript Received December 20, 1995⊗

ABSTRACT: The structures of the (*R*)- and (*S*)-α-(*N*^{2}-guanyl)styrene oxide adducts at X^6 in d(GGCAGXTGGTG)·d(CACCACCTGCC), encompassing codon 12 of the human *n-ras* protooncogene (underlined), were refined from ^{1}H NMR data. These were the R(12,2) and S(12,2) adducts. For the R(12,2) adduct, upfield chemical shifts were observed for the T^7 H6, H1′, and N3H resonances. At 30 °C, $^{R\text{-}SO}G^6$ N1H, T^7 N3H, and T^{10} N3H disappeared due to exchange with solvent. For the S(12,2) adduct, $^{S\text{-}SO}G^6$ H1′ shifted upfield 0.33 ppm, but all imino resonances were observed. The styrene methylene protons were nonequivalent for both adducts, suggesting hydrogen bonding between the hydroxyl and C^{18} O2 or O4′ in the R(12,2) adduct and C^{17} O2 in the S(12,2) adduct. The styrene aromatic protons appeared as three signals in the R(12,2) adduct and as two signals in the S(12,2) adduct, suggesting rapid rotation of the styrene ring on the NMR time scale. NOE data revealed that the phenyl ring was oriented in the 3′-direction relative to $^{R\text{-}SO}G^6$ for the R(12,2) adduct and in the 5′-direction relative to $^{S\text{-}SO}G^6$ for the S(12,2) adduct. A total of 253 and 221 interproton distances were obtained from relaxation matrix analyses of the R(12,2) and S(12,2) adducts, respectively. NOE-restrained molecular dynamics calculations converged with root mean square deviations of 0.8−1.2 Å for the R(12,2) adduct and 0.82−1.4 Å for the S(12,2) adduct. Complete relaxation matrix analyses of the nine inner base pairs yielded sixth root residual indices between calculated and experimental NOE intensities of 8.8×10^{-2} for the R(12,2) adduct and 7.9×10^{-2} for the S(12,2) adduct. The refined structure for the R(12,2) adduct showed a 0.4 Å increase in the stretch of $^{R\text{-}SO}G^6$·C^{17} and T^7·A^{16}, and a 1−2 Å widening of the minor groove at and adjacent to the SO lesion, with the styrene ring oriented edgewise in the minor groove. Smaller minor groove disturbances were observed for the S(12,2) adduct, which had the styrene ring oriented flat in the minor groove. No DNA bending was predicted by the calculated structures.

Styrene, a mutagen in prokaryotes (de Meester et al., 1977; Wade et al., 1978) and eukaryotes (Bonatti et al., 1978), and possibly in humans (Ott et al., 1980; Hodgson & Jones, 1985; Matanoski & Schwarts, 1987; Wong, 1990), induces sister chromosome exchange and aberrations in human lymphocytes *in vitro* (Norppa et al., 1980, 1981). The genotoxicity is believed to be due to cytochrome P_{450}-mediated metabolism to styrene oxide, SO[1] (Harris et al., 1986; Foureman et al., 1989; Elovaara et al., 1991; Guengerich et al., 1991; Guengerich, 1992; Nelson et al., 1993; Nakajima et al., 1994a,b). This oxide reacts *in vitro* to form adducts at a number of nucleophilic sites in DNA, including the *R*- and *S*-enantiomers at the exocyclic amino group of guanine (Savela & Hemminki, 1986).

The site-specific adduction of DNA by reactive electrophiles is commonly postulated to be the initiating step in chemical carcinogenesis. Ultimately, adducts are believed to induce mutations during DNA replication or repair (Miller, 1970, 1978). Both adduction of DNA by electrophilic agents (Muench et al., 1983; Refolo et al., 1985; Boles & Hogan, 1986; Marien et al., 1987; Benasutti et al., 1988; Kootstra et al., 1989; Moyer et al., 1989; Osborne, 1990; Dittrich & Krugh, 1991a,b; Margulis et al., 1993) and subsequent biological processing of DNA lesions, including repair (Zarbl et al., 1985; Topal et al., 1986; Topal, 1988; Voigt et al., 1989; Voigt & Topal, 1990), and either correct or incorrect replication resulting in mutations (Koffel-Schwartz et al., 1984; Gentil et al., 1986; Marien et al., 1989; Hoffmann & Fuchs, 1990; Lambert et al., 1992a,b; Levy et al., 1992; Latham et al., 1993; Rodriguez & Loechler, 1993b; Chary et al., 1995), are modulated by sequence.

Mutations in particular DNA sequences seem to be involved in tumorigenesis. Active oncogenes have been found in a number of human tumors (Shih et al., 1981; Krontiris & Cooper, 1981; Perucho et al., 1981; Pulciani et al., 1982); often these are members of the *ras* protooncogene family (Cooper, 1982; Land et al., 1983). Activation of *ras*

† This research was supported by the NIH: Grant ES-05355 (M.P.S.) and Grant ES-05509 (T.M.H.). Funding for the AMX-500 NMR spectrometer was supplied by the NIH shared instrumentation program, Grant RR-05805, and the Vanderbilt Center in Molecular Toxicology, Grant ES-00267.

* Author to whom correspondence should be addressed.

‡ Present address: Janssen Research Foundation, Welsh and McKean Roads, Spring House, PA 19477.

⊗ Abstract published in *Advance ACS Abstracts,* March 1, 1996.

[1] Abbreviations: DNA, deoxyribonucleic acid; DSS, sodium 4,4-dimethyl-4-silapentanesulfonate; EDTA, ethylenediaminetetraacetic acid; HPLC, high-pressure liquid chromatography; NMR, nuclear magnetic resonance; NOE, nuclear Overhauser enhancement; NOESY, two-dimensional NOE spectroscopy; PAH, polycyclic aromatic hydrocarbon; ppm, parts per million; R-Y-R, purine−pyrimidine−purine; SO, styrene oxide; TPPI, time-proportional phase increment; TOCSY, total homonuclear correlated spectroscopy; 1D, one dimensional; 2D, two dimensional.

0006-2960/96/0435-4334$12.00/0

is a consequence of mutations within a limited number of codons of the gene product, including codon 12 [reviewed by Barbacid (1987)]. Therefore, understanding adduct-induced perturbations of DNA containing the *ras* codon 12 sequence, and in which potential mutations are associated with tumorigenesis, is crucial. The guanine-rich codon 12 sequence may be unusually prone to benzo[*a*]pyrene adduct formation at guanine N2 (Dittrich & Krugh, 1991a). It seems plausible, although it is not established, that SO generated *in vivo* might also target the codon 12 sequence.

The structure refinement of the *ras12* oligodeoxynucleotide d(GGCAGGTGGTG)·d(CACCACCTGCC)[2] (Zegar & Stone, 1996), in which the underlined nucleotides represent the codon 12 sequence, revealed a B-type conformation, with local variations (Calladine, 1982) associated with three purine−pyrimidine−purine (R-Y-R) steps in the coding strand: $G^2 \rightarrow C^3 \rightarrow A^4$, $G^6 \rightarrow T^7 \rightarrow G^8$, and $G^9 \rightarrow T^{10} \rightarrow G^{11}$. The $G^6 \rightarrow T^7 \rightarrow G^8$ step was of particular interest since it involved the second and third (wobble) nucleotides of codon 12. These R-Y-R steps were reflected in the calculated roll angles, slide, and rise parameters from the refined *ras12* structures. The significance of sequence-dependent structural variations within the codon 12 region with regard to adduct-induced mutagenesis remains to be determined. These could alter the propensity for adduction at this site, e.g., by inducing sequence-specific changes in the corresponding transition state energy barriers for reaction with specific electrophilic species (Warpehoski & Hurley, 1988) or by inducing sequence-specific changes in the binding equilibria for electrophiles (Muench et al., 1983; Boles & Hogan, 1984). Likewise, in the adducted DNA, perturbations in the R-Y-R base-step geometry at codon 12 could influence the propensity toward mutation or repair, in a site-specific and adduct-specific manner.

Stereochemistry modulates adduct conformation at guanine N2, as revealed for diastereomeric benzo[*a*]pyrene adducts (De Los Santos et al., 1992). Subsequent studies of benzo[*a*]pyrene (Cosman et al., 1994a,b; Fountain & Krugh, 1995) and 5-methylchrysene (Cosman et al., 1995b) adducts at guanine N2 substantiated this observation. Stereospecific differences in the processing of PAH lesions (Shibutani et al., 1993; Wei et al., 1994) suggested the existence of a relationship between the configurations of particular adducts and their biological fate. Stereospecific differences in structure for PAH (Cosman et al., 1993, 1995a; Schurter et al., 1995a,b) and SO (Feng et al., 1995) adducts,[3] and as well, for the processing of PAH (Cheh et al., 1994; Christner et al., 1994; Chary et al., 1995) and SO (Latham et al., 1993, 1995) adducts at adenine N6 have been documented.

Scheme 1: R(12,1) and R(12,2) Oligodeoxynucleotides, where R or S = (*R*)- or (*S*)-α-(*N*^{2}-Guanyl)styrene Oxide Adduct (Bottom)

***ras* codon**

```
          11      12      13
5'-G1 |G2 C3 A4 |G5 R6 T7 |G8 G9 T10|G11-3'
3'-C22|C21G20T19|C18C17A16|C15C14A13|C12-5'
```

***ras* codon**

```
          11      12      13
5'-G1 |G2 C3 A4 |G5 S6 T7 |G8 G9 T10|G11-3'
3'-C22|C21G20T19|C18C17A16|C15C14A13|C12-5'
```

Scheme 2: Structures of the (*R*)- and (*S*)-α-Styrene Oxide Adducts at Guanine N2

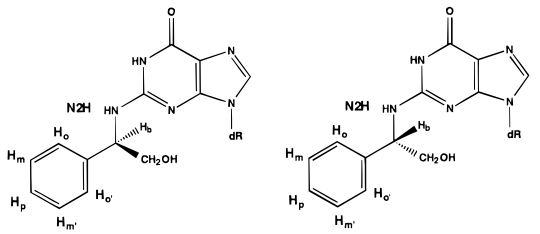

The present work focuses on the effect of altering the stereochemistry of the α-(*N*^{2}-guanyl)styrene oxide adduct at position G^6 in the *ras12* oligodeoxynucleotide. Solution conformations of the stereoisomeric R(12,2) and S(12,2) adducts, as obtained from ^{1}H NMR spectroscopy (Schemes 1 and 2), are compared. NOESY and TOCSY spectra are used to assign ^{1}H resonances. Interproton distance restraints obtained from NOESY spectra produce refined solution structures through restrained MD simulation incorporating simulated annealing, followed by full relaxation matrix back-calculation of the spectra (Keepers & James, 1984; Havel & Wuthrich, 1985; Wuthrich, 1986; Nilsson et al., 1986; Borgias & James, 1990; Madrid et al., 1991). The refined structures that emerge from the calculations are in the B-family, with discernible differences at and adjacent to the site of modification. The results reveal the influence of adduct stereochemistry in determining the orientation of styrene oxide adducts at guanine N2, with the *R*-diastereomer being oriented in the 3′-direction while the *S*-diastereomer is oriented in the 5′-direction from the lesion site. The accommodation of the *R*-diastereomer within the minor groove requires greater distortion of the *ras12* oligodeoxynucleotide, which appears to be related to steric crowding when the phenyl ring is oriented in the 3′- as opposed to the 5′-direction. The R(12,2) and S(12,2) styrene oxide structures provide a model system for the study of site-directed mutagenesis and replication studies within the coding sequence of the human *n-ras* protooncogene at codon 12.

MATERIALS AND METHODS

Materials. The oligodeoxynucleotide d(CACCACCTGCC) was purchased from the Midland Certified Reagent Co. (Midland, TX). The site-specific incoporation of styrene into the *ras12* sequence was accomplished by reaction of the enantiomeric phenylglycinols with the *ras12* oligodeoxynucleotide containing 2-fluoroinosine deoxyriboside at the desired target site. This was conceptually similar to an

[2] The oligonucleotides discussed in this paper do not have terminal phosphate groups—we abbreviate the nomenclature for oligonucleotides by leaving out the phosphodiester linkage. A, C, G, T, and X refer to mononucleotide units; X is the (*S*)- or (*R*)-α-styrene oxide modified nucleotide. A right superscript refers to numerical position in the oligonucleotide sequence starting from the 5′-terminus of chain A and proceeding to the 3′-terminus of chain A and then from the 5′-terminus of chain B to the 3′-terminus of chain B. C2, C5, C6, C8, C1′, C2′, etc. represent specific carbon nuclei. H2, H5, H6, H8, H1′, H2′, H2″, etc. represent the protons attached to these carbons.

[3] B. Feng, M. Voehler, L. Zhou, M. Passarelli, C. M. Harris, T. M. Harris, and M. P. Stone, "Major Groove (*S*)-α-(*N*^{6}-Adenyl)styrene Oxide Adducts in an Oligodeoxynucleotide Containing the Human *N-ras* Codon 61 Sequence: Conformations of the S(61,2) and S(61,3) Sequence Isomers from ^{1}H NMR", manuscript submitted for publication.

approach used to prepare (*R*)- and (*S*)-α-(N^6-adenyl)styrene oxide-adducted oligodeoxynucleotides (Harris et al., 1991,1994) and enabled large-scale production of (*R*)- and (*S*)-α-(N^2-guanyl)styrene oxide adducted oligodeoxynucleotides (DeCorte et al., 1996). The modified oligodeoxynucleotides were purified by HPLC using a reverse-phase semipreparative column (PRP-1; Hamilton Co., Reno, NV) equilibrated with 10 mM ethylenediamineacetate (pH 7.0). The oligodeoxynucleotides were eluted using a gradient consisting of 0−20% acetonitrile in 20 min. The DNA was lyophilized and desalted on Sephadex G-25 (Pharmacia-P.L. Biochemicals, Inc., Piscataway, NJ).

Preparation of NMR Samples. The concentration of d(GGCAGGTGGTG) was determined from the calculated extinction coefficient at 260 nm of 1.09×10^5 M^{-1} cm^{-1} (Borer, 1975), while concentrations of d(GGCAG$^{R\text{-}SO}$GTGGTG) and d(GGCAG$^{S\text{-}SO}$GTGGTG) were determined from the calculated extinction coefficient at 260 nm of 9.24×10^4 M^{-1} cm^{-1}. The complementary oligodeoxynucleotides were mixed at approximately equal molar ratios in 10 mM NaH_2PO_4, 0.1 M NaCl, and 50 μM Na_2EDTA, at pH 6.9. The mixtures were heated to 85 °C for 5 min followed by cooling to room temperature to anneal the strands. DNA grade Bio-Gel hydroxylapatite (Bio-Rad Laboratories, Richmond, CA) (15 cm × 3.0 cm), eluted with a NaH_2PO_4 gradient from 10 to 200 mM (pH 6.9), was used for the separation of double-stranded from single-stranded DNA. The duplexes were lyophilized, resuspended in 1 mL of H_2O, and desalted on Sephadex G-25 (70 cm × 1.5 cm). The samples were lyophilized and dissolved in 0.5 mL of NMR buffer [0.1 M NaCl, 5×10^{-5} M Na_2EDTA, 0.01 M NaH_2PO_4 (pH 6.9)]. The final concentrations of the samples were determined to be 2.5 mM in strand concentration. Strand stoichiometries were assayed by HPLC.

Nuclear Magnetic Resonance. Spectra were recorded at a ^1H frequency of 500.13 MHz. The samples used for examination of nonexchangeable protons were lyophilized three times from 99.96% D_2O and suspended into 0.5 mL of NMR buffer containing 99.996% D_2O. The samples used for examination of exchangeable protons were dissolved in 0.5 mL of NMR buffer containing 9:1 H_2O:D_2O. The spectra were referenced to the water resonance at 4.72 ppm at 30 °C or 4.97 ppm at 10 °C. Phase-sensitive NOESY spectra used for the resonance assignments were recorded using the TPPI method for phase cycling. A mixing time of 400 ms was used. In the d_1 dimension, 1024 real data points were collected, with 32 acquisitions per FID with a 1.5 s relaxation delay; 2048 real data points were used in the d_2 dimension. The residual water resonance was saturated during the relaxation delay and the mixing period. Data were zero-filled in the d_1 dimension to give a matrix of 2K × 2K real points. A sine-bell apodization function with a 90° phase shift and a skew factor of 0.7 was used in the d_1 and d_2 dimensions. Phase-sensitive NOESY experiments in 9:1 H_2O:D_2O were performed using a jump return 1−1 sequence for water suppression as the read pulse (Bax et al., 1987; Sklenar et al., 1987). Convolution difference was used during processing to minimize the residual water signal (Marion et al., 1989). The NOE mixing time was 250 ms. In the d_1 dimension, 512 data points were collected, with 64 scans per FID; the relaxation delay was 1.5 s. In the d_2 dimension, 2K data points were utilized. These experiments were carried out at 10 °C. Phase-sensitive TOCSY spectra were recorded using a 105 ms MLEV17 (Bax & Davis, 1985) spin lock at 2 G for mixing (phase cycling was done according to the TPPI method). These experiments were carried out at 30 °C. The data were transferred to Iris 4D workstations (Silicon Graphics, Inc., Mountain View, CA) and processed using FELIX (Biosym Technologies, San Diego, CA).

NMR Distance Restraints. Classical B-DNA and A-DNA (Arnott & Hukins, 1972) were used as the reference structures. The initial DNA models were constructed by bonding C1 of styrene to N2 of guanine using INSIGHTII (Biosym Technologies, San Diego, CA). Partial charges on the styrene ring were obtained from those assigned to phenylalanine from the CHARMM force field. These were energy minimized for 500 iterations by the conjugate gradient method to give the starting structures IniA and IniB. NOESY spectra at mixing times of 100, 150, and 250 ms [R(12,2) adduct] and 150, 250, and 350 ms [S(12,2) adduct] were acquired within a single 3-day period without removing the sample from the spectrometer or changing the experimental conditions. The NOESY pulse program was modified to eliminate artifacts arising from zero-quantum coherence and *zz* terms observed at short mixing times. A systematically shifted composite 180° pulse was implemented within the mixing period, and composite 90° pulses were used in place of the second and third 90° pulses in the standard pulse sequence (Bodenhausen et al., 1984). Footprints were drawn around the NOE cross peaks for the NOESY spectrum measured at a mixing time of 250 ms [R(12,2) adduct] and 350 ms [S(12,2) adduct] using FELIX. The same set of footprints was applied to spectra measured at other mixing times. Cross peak intensities were determined by volume integration of the areas under the footprints. The intensities were combined as necessary with intensities generated from complete relaxation matrix analysis of a starting DNA structure to generate a hybrid intensity matrix. MARDIGRAS (Borgias & James, 1990) was used to iteratively refine the hybrid matrix to optimize the agreement with experimental NOE intensities. Calculations using IniA and IniB, three mixing time NOE experiments (100, 150, and 250 ms), and four DNA correlation times (2, 3, 4, and 5 ns), yielded 24 sets of distances, which were averaged. For the S(12,2) adduct, only the B-starting model was used. Volumes measured from three NOESY experiments at 150, 250, and 350 ms mixing times and correlation times of 3, 4, and 5 ns yielded nine sets of internuclear distances. These were averaged.

Molecular Dynamics and Simulated Annealing. A detailed description of the molecular dynamics and simulated annealing protocol used in these studies is provided in the Supporting Information. INSIGHTII was used to build the starting structures and for molecular visualization. All potential energy minimization and restrained MD calculations were performed using X-PLOR (Brunger, 1992). This was derived from CHARMM (Brooks et al., 1983) and adapted for restrained MD calculations of nucleic acids. The empirical energy function (Nilsson et al., 1986) was developed especially for nucleic acids and treated all hydrogens explicitly. It consisted of energy terms for bonds, bond angles, torsion angles, tetrahedral and planar geometry, hydrogen bonding, and nonbonded interactions including van der Waals and electrostatic forces. The van der Waals energy term was approximated using the Lennard-Jones potential

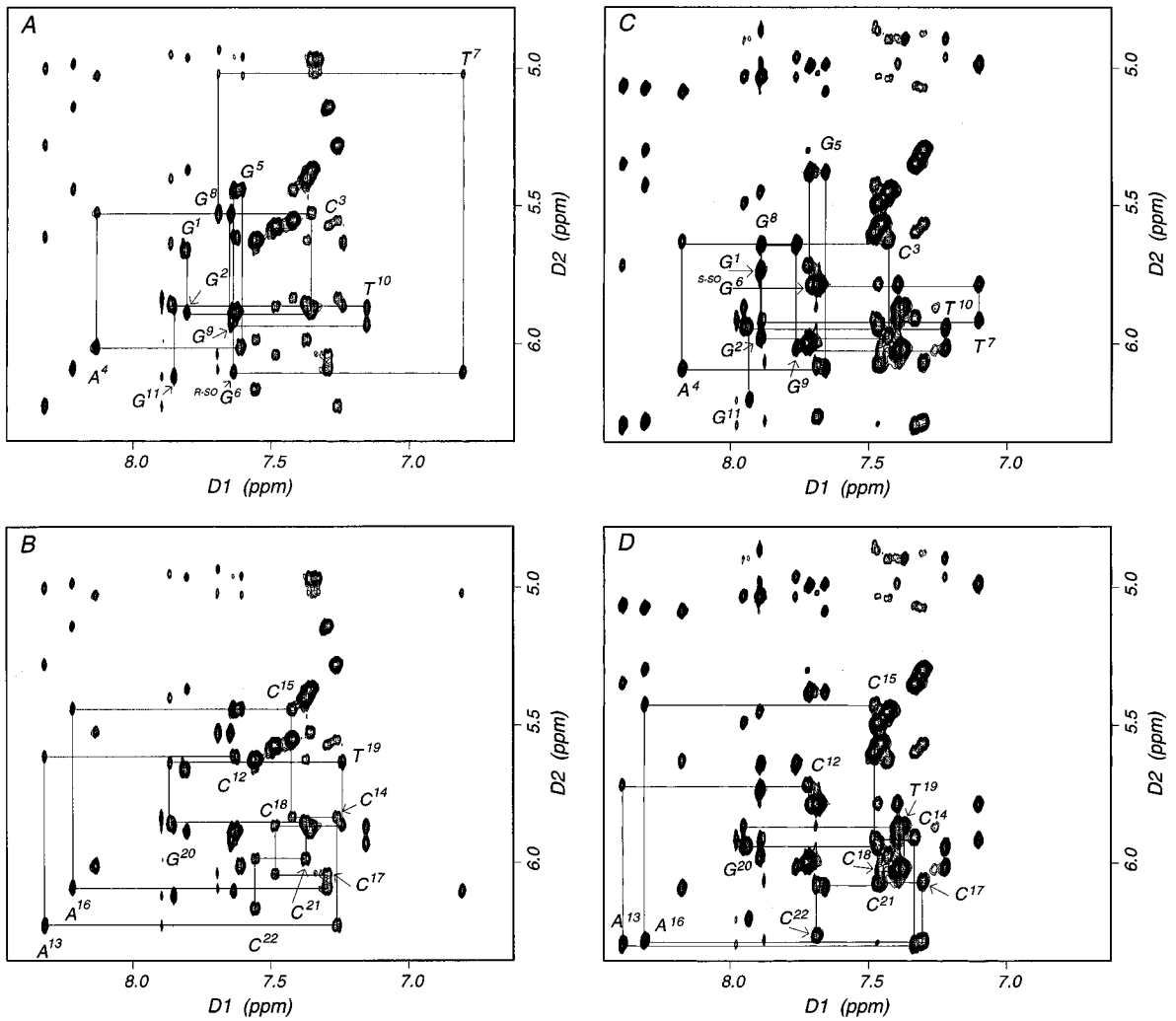

FIGURE 1: Expanded plot of a phase-sensitive NOESY spectrum at 250 ms mixing time showing the sequential NOEs from the aromatic to H1′ protons: (A) the modified strand of the R(12,2) duplex; (B) the unmodified strand of the R(12,2) duplex; (C) the modified strand of the S(12,2) duplex; (D) the unmodified strand of the S(12,2) duplex. The base positions are indicated at the intranucleotide aromatic to sugar H1′ NOE cross peak.

energy function. The electrostatic term used the Coulomb function, based on full partial charges and a distance-dependent dielectric constant of 4. The nonbonded pair list was updated if any atom moved more than 0.5 Å, and the cutoff radius for nonbonded interactions was 11 Å. The effective energy function was composed of two terms describing distance and dihedral restraints, which were in the form of a square well potential (Clore et al., 1986). All bond lengths involving hydrogen were kept fixed with the SHAKE algorithm (Ryckaert et al., 1977) during MD calculations. All calculations were performed *in vacuo* without explicit counter ions. The integration time step used in the molecular dynamics calculations was 1 fs. Structure coordinates were archived every 0.1 ps. Back-calculation of NMR data was performed using CORMA (Keepers & James, 1984). The refined structures were examined using DIALS AND WINDOWS 1.0 (Ravishankar et al., 1989). However, locating local energy minima among a large (>100) ensemble of MD-emergent structures or the identification of conformationally distinct clusters of structures which could simultaneously satisfy the NMR restraints (Gupta et al., 1993) was not attempted.

RESULTS

Spectral Assignments. (a) Nonexchangeable Protons. Sequential assignments of the nonexchangeable protons were determined at 30 °C in the standard manner (Hare et al., 1983; Feigon et al., 1983). The H2′ and H2″ sugar protons were assigned from NOEs with the H1′ sugar protons of the same residue, on the basis of the assumption that, for a B-like DNA, the H1′-H2″ distances were shorter than the H1′-H2′ distances. Therefore, the stronger cross peaks were assigned to the H2″ protons. These assignments were corroborated by TOCSY and DQF-COSY data, which were used to assign the remainder of the deoxyribose sugar protons. The H5′/H5″ resonances were identified for the R(12,2) oligomer but not separately assigned. They were not identified for the S(12,2) oligomer. A number of these resonances overlapped, which made unambiguous assignments impossible. The adenine H2 protons were assigned from weak cross peaks to the H1′ protons of the adjacent 3′-nucleotides.

The sequential assignments for both strands of each oligomer were obtained without interruptions (Figure 1). The notable feature observed in this region of the spectrum for the modified strand of the R(12,2) duplex was an upfield chemical shift for T^7 H6 and T^7 H1′, relative to the

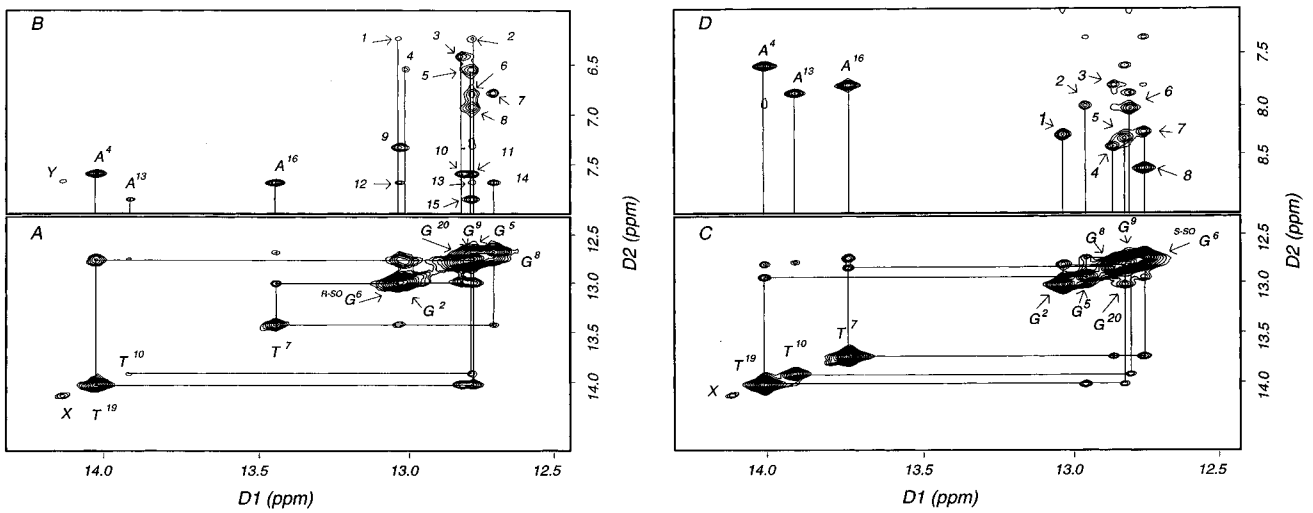

FIGURE 2: (A) The R(12,2) adduct. NOEs for imino protons of base pairs $G^2 \cdot C^{21} \rightarrow T^{10} \cdot A^{13}$ at 350 ms mixing time. (B) The R(12,2) adduct. NOEs between T^{19}, T^{10}, and T^7 N3H and A^4, A^{13}, and A^{16} H2. Labeled cross peaks: 1, $^{R\text{-}SO}G^6$ N1H-C^{17} NH_{2b}; 2, G^5 N1H-$C^{17}NH_{2b}$; 3, G^{20} N1H-C^3 NH_{2b}; 4, G^2 N1H-C^{21} NH_{2b}; 5, G^9 N1H-C^{14} NH_{2b}; 6, G^9 N1H-C^{15} NH_{2b}; 7, G^8 N1H-C^{15} NH_{2b}; 8, G^5 N1H-C^{18} NH_{2b}; 9, $^{R\text{-}SO}G^6$ N1H-styrene $H_{o,o'}$; 10, G^{20} N1H-A^4 H2; 11, G^5 N1H-A^4 H2; 12, $^{R\text{-}SO}G^6$ N1H-A^{16} H2; 13, G^9 N1H-A^{16} H2 (spin diffusion); 14, G^8 N1H-A^{16} H2; 15, G^9 N1H-A^{13} H2. (C) The S(12,2) adduct. NOEs for imino protons of base pairs $G^2 \cdot C^{21} \rightarrow T^{10} \cdot A^{13}$ at 250 ms mixing time. (D) The S(12,2) adduct. NOEs between T^{19}, T^{10}, and T^7 N3H and A^4, A^{13} and A^{16} H2. Labeled cross peaks: 1, G^2 N1H-C^{21} NH_{2b}; 2, G^5 N1H- C^{17} NH_{2b}; 3, G^8 N1H-A^{16} H2; 4, G^8 N1H-C^{15} NH_{2b}; 5, G^{20} N1H- C^3 NH_{2b}; 6, G^9 N1H-C^{14} NH_{2b}; 7, $^{S\text{-}SO}G^6$ N1H-C^{17} NH_{2b}; 8, $^{S\text{-}SO}G^6$ N1H-$^{S\text{-}SO}G^6$ 2-NH. All spectra were obtained at 10 °C. The resonances labeled X and Y were unidentified.

unmodified oligomer (Zegar & Stone, 1996). With the exception of T^7 H6, the aromatic protons of the purine and pyrimidine bases resonated within the expected range of chemical shifts, ranging from 7.1 to 8.4 ppm. The relative positions of G^5 H8 and $^{R\text{-}SO}G^6$ H8 interchanged with respect to the unmodified oligomer, with $^{R\text{-}SO}G^6$ H8 shifted further downfield in the modified oligomer. There was some spectral overlap, involving G^1 H8 and G^2 H8, and G^5 H8 and $^{R\text{-}SO}G^6$ H8, which were nearly isonchronous. In the complementary strand, the aromatic H6 protons of nucleotides C^{14} and T^{19}, and of C^{15}, C^{18}, and C^{21} were nearly isonchronous. The three sets of sequential cytosine aromatic resonances, $C^{14} \rightarrow C^{15}$, $C^{17} \rightarrow C^{18}$, and $C^{21} \rightarrow C^{22}$, exhibited a characteristic pattern, with the 5′-neighbor cytosine in each case resonating at higher field than the 3′-neighbor cytosine. With the exception of T^7 H1′, the anomeric protons resonated within the expected range of 5.4−6.4 ppm.

For the S(12,2) oligomer, a notable spectral feature was the upfield shift for G^5 H1′, relative to the same resonance in the unmodified oligomer (Zegar & Stone, 1996). This, combined with the appearance of T^7 H6 and H1′ in the normal spectral region and a downfield shift of G^8 H8, created a greater overlap problem with the S(12,2) adduct spectral data. As in the case of the R(12,2) oligomer, $^{S\text{-}SO}G^6$ H8 shifted further downfield than G^5 H8, relative to the unmodified oligomer. Spectral overlap involved G^1 H8, G^2 H8, and G^8 H8, and G^5 H8 and $^{S\text{-}SO}G^6$ H8, which were nearly isonchronous. In the complementary strand, the H6 protons of nucleotides C^{14}, C^{17}, and T^{19}, and of C^{15}, C^{18}, and C^{21}, were nearly isonchronous. Similar to what was observed for the R(12,2) duplex, the three sets of sequential cytosine aromatic resonances, $C^{14} \rightarrow C^{15}$, $C^{17} \rightarrow C^{18}$, and $C^{21} \rightarrow C^{22}$, had the 5′-neighbor cytosine resonating at higher field than the 3′-neighbor cytosine. Tables 1S and 2S in the Supporting Information list the chemical shifts of the nonexchangeable protons.

(b) Exchangeable Protons. Assignments of the imino and amino protons for the R- and S(12,2) oligodeoxynucleotides were carried out from NOESY spectra measured in 90% H_2O (Boelens et al., 1985). Tile plots of the imino and amino regions of the R(12,2) and S(12,2) adducts are shown in Figure 2. The non-hydrogen-bonded amino protons of cytosines (NH_{2a}) were assigned from their connectivities to H5 protons of cytosines. The hydrogen-bonded amino resonances of cytosine (NH_{2b}) were then assigned from their cross peaks to NH_{2a}. With the exception of the 5′-terminal cytosine, two resonances were observed for each set of cytosine amino protons. $^{R\text{-}SO}G^6$ 2-NH was assigned from NOEs to $^{R\text{-}SO}G^6$ N1H and T^7 N3H. Similarly, $^{S\text{-}SO}G^6$ 2-NH was assigned from NOEs to G^5 N1H, $^{S\text{-}SO}G^6$ N1H, and T^7 N3H. The remainder of the guanine amino protons were not assigned due to exchange broadening. The chemical shifts of the exchangeable protons are listed in Tables 3S and 4S in the Supporting Information. Compared to the unmodified duplex, the guanine imino protons were better resolved.

For the R(12,2) oligomer, two well-resolved resonances were observed between 13.4 and 14.0 ppm at 10 °C (Figure 2A). The resonance at 14.0 ppm was assigned to T^{19} N3H from a cross peak to A^4 H2. The resonance at 13.4 ppm was assigned to T^7 N3H from a cross peak to A^{16} H2 and was approximately 0.6 ppm upfield of the other thymine imino resonances. In the spectrum shown in Figure 2A, T^{10} N3H was exchange broadened and was identified on the basis of a cross peak to A^{13} H2. The cluster of resonances located between 12.5 and 13.2 ppm was identified as guanine imino protons, with the exception of G^1 and G^{11} N1H, which were exchange broadened. A notable feature from this region was the downfield chemical shift of $^{R\text{-}SO}G^6$ N1H, relative to G^6 N1H in the unmodified oligomer. The imino protons of G^5, G^9, and G^{20} were nearly isonchronous and were identified on the basis of NOEs to amino protons from the complementary cytosines, C^{18}, C^{14}, and C^3, respectively.

The imino proton region of the spectrum for the S(12,2) oligomer at 10 °C is shown in Figure 2B. Three well-resolved resonances were observed between 13.5 and 14.0

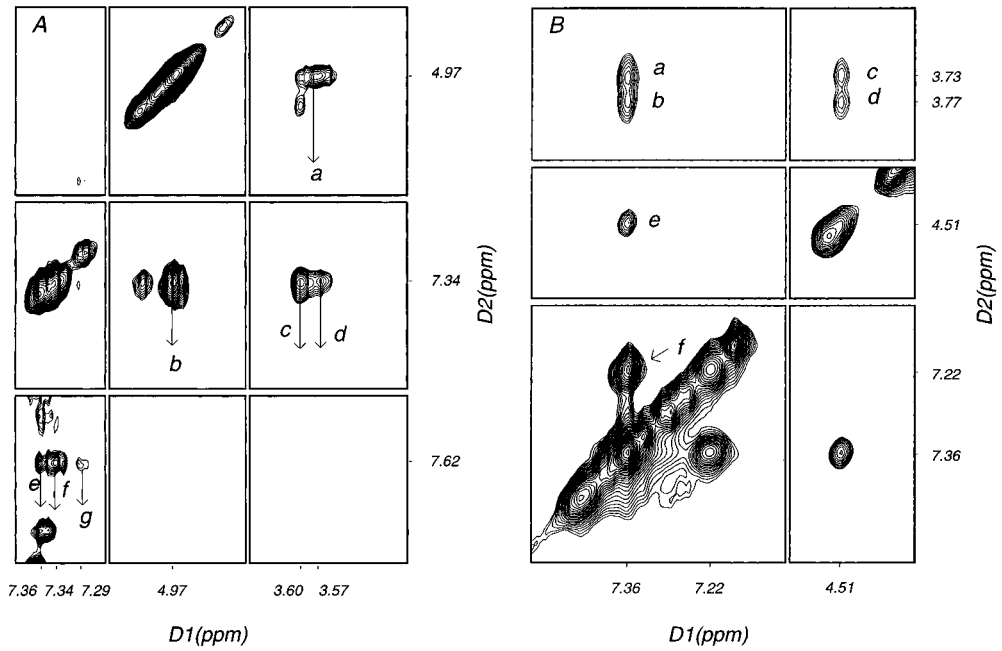

FIGURE 3: Tile plots from NOESY spectra showing styrene resonances. (A) The R(12,2) adduct: a, H_b-$H_{\beta',\beta''}$; b, H_b-$H_{o,o'}$; c, d, $H_{\beta',\beta''}$-$H_{o,o'}$. Additional cross peaks e, f, and g, A^{16} H2-$H_{m,m'}$, -$H_{o,o'}$, and -H_p. (B) The S(12,2) adduct: a, $H_{\beta'}$-$H_{o,o',m,m'}$; b, $H_{\beta''}$-$H_{o,o',m,m'}$; c, $H_{\beta'}$-H_b; d, $H_{\beta''}$-H_b; e, H_b-$H_{o,o',m,m'}$; f, H_p-$H_{o,o',m,m'}$.

ppm. These were assigned to T^7, T^{10}, and T^{19} N3H from cross peaks to the H2 protons of the complementary adenines. The resonances located between 12.5 and 13.0 ppm were identified as guanine N1H protons. Again, G^1 and G^{11} N1H were exchange broadened. The imino proton of $^{S\text{-}SO}G^6$ was closer to the resonance frequency observed for the unmodified *ras12* oligomer than that of the R(12,2) oligomer. Similar to the R(12,2) oligomer, the imino protons of G^5, G^9, and G^{20} were nearly isonchronous and were identified on the basis of NOEs to amino protons of the complementary cytosines, C^{18}, C^{14}, and C^3, respectively.

(c) Styrene Protons and Styrene−DNA NOE Connectivities. (a) The R(12,2) Adduct. The R(12,2) styrene resonances from a NOESY spectrum obtained at 350 ms mixing time are shown in Figure 3A. The aromatic resonances of the styrene ring were clustered and appeared as three signals between 7.29 and 7.36 ppm. In 1D spectra, these resonances were overlapped with C^3, C^{14}, and C^{17}. A strong cross peak between two resonances at 3.57 and 3.60 ppm and one resonance at 4.97 ppm (peak a) identified the methylene and benzylic protons, respectively. The benzylic proton, H_b, showed a strong cross peak(s) to a resonance at 7.34 ppm (peak b), which was assigned to one or both ortho protons, $H_{o,o'}$, of SO. A second-order NOE was observed between this ortho proton and the methylene protons (peaks c and d). Furthermore, A^{16} H2 showed weak NOE cross peaks to three resonances at 7.29, 7.34, and 7.36 ppm. The strongest of these was to the 7.34 ppm resonance that was assigned to $H_{o,o'}$, and the weaker connectivities to the resonances at 7.36 and 7.29 were attributed to the meta and para protons ($H_{m,m'}$ and H_p) of the styrene ring, respectively. Further support for the assignment of the phenyl protons is given in the following discussion.

There were a total of 23 NOE cross peaks between the styrene protons and the nonexchangeable and exchangeable DNA protons for the R(12,2) duplex. Of these NOEs, 21 are shown in Figure 4 A. The individual methylene protons of SO exhibited a characteristic set of NOEs to DNA protons. The downfield methylene resonance at 3.60 ppm showed NOEs to G^5 N1H, $^{R\text{-}SO}G^6$ N1H, $^{R\text{-}SO}G^6$ 2-NH, and T^7 H1′ and H4′ (peaks a−c, e, f), all of which are located in the modified strand of the DNA. It was likely that the T^7 H1′ and H4′ cross peaks reflected spin diffusion. However, these cross peaks may also be consistent with the adduct-induced out-of-plane distortion of T^7, predicted by the refinement calculations discussed in a following section. The upfield methylene resonance at 3.57 ppm showed a strong NOE to C^{18} H1′ (peak d), and weaker NOEs to C^{18} H5′/H5″ and T^{19} H5′/H5″ (peaks g and h), on the complementary strand. The T^{19} H5′/H5″ cross peaks were judged to have arisen from spin diffusion. This identified the 3.6 ppm resonance as $H_{\beta'}$ and the 3.57 ppm resonance as $H_{\beta''}$. A strong cross peak was observed between $^{R\text{-}SO}G^6$ 2-NH and the resonance at 7.34 ppm (peak k), which established that the latter must arise from an ortho proton on the styrene ring. Cross peaks were also observed between $H_{o,o'}$ and T^7 H1′ (peak n) and between $H_{o,o'}$ and C^{17} H1′ (peak m). In addition, cross peaks were observed between $^{R\text{-}SO}G^6$ H4′ and H_p (peak o) and $H_{o,o',m,m'}$ (peak p). H_p and $H_{o,o'}$ also showed strong cross peaks to T^7 H4′, C^{18} H4′ (peaks q and r), G^8 H5′/H5″ (peaks s and t), and T^{19} H5′/H5″ (peak u). These NOEs established the 3′-orientation of the SO phenyl ring relative to $^{R\text{-}SO}G^6$.

(b) The S(12,2) Adduct. In Figure 3B, the resonance at δ 4.51 ppm was assigned to H_b since it showed a strong NOE to the methylene protons of the CH_2OH group (peaks c and d) in both TOCSY and NOESY spectra. The methylene protons were located at δ 3.73 and 3.77 ppm. The resonance at δ 3.77 ppm was assigned to $H_{\beta''}$ since it showed a stronger cross peak to A^{16} H2. The resonances of the styrene ring were not resolved. Two resonances of area 1:4 at δ 7.22 and 7.36 ppm were observed. The resonance at δ 7.22 ppm was assigned to H_p since, in all possible orientations, both $H_{o'}$ and $H_{m'}$ were expected to exhibit strong NOEs to $^{S\text{-}SO}G^6$ H1′. The δ 7.22 ppm resonance did not exhibit this NOE, while the δ 7.36 ppm resonance did. Since only one strong cross peak was observed between H_b and the resonance at δ

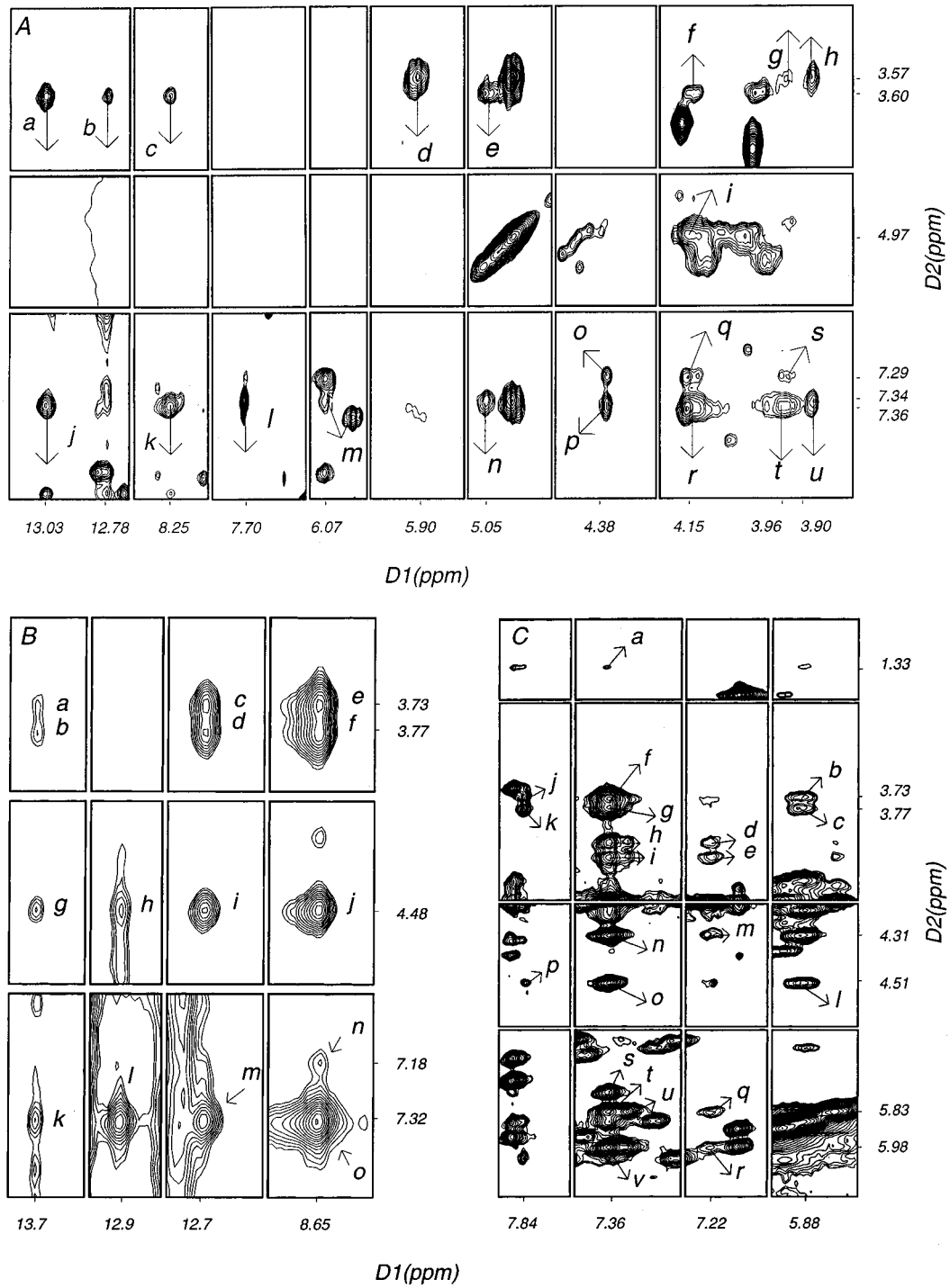

FIGURE 4: NOE cross peaks between styrene oxide and DNA protons. (A) The R(12,2) adduct: a, $H_{\beta'}$-$^{R\text{-}SO}G^6$; b, $H_{\beta'}$-G^5 N1H; c, $H_{\beta'}$-$^{R\text{-}SO}G^6$ 2-NH; d, $H_{\beta''}$-C^{18} H1′; e, $H_{\beta'}$-T^7 H1′ (spin diffusion); f, $H_{\beta'}$-T^7 H4′ (spin diffusion); g, $H_{\beta''}$-T^{19} H5′/H5″; h, $H_{\beta''}$-C^{18} H5′/H5″ (spin diffusion); i, H_b-T^7 H4′; j, $H_{o,o'}$-$^{R\text{-}SO}G^6$ N1H; k, $H_{o,o'}$-$^{R\text{-}SO}G^6$ 2-NH; l, $H_{o,o',m,m'}$-A^{16} H2; m, H_o-C^{17} H1′; n, H_o-T^7 H1′; o, H_p-G^8 H4′; p, $H_{o,o',m,m'}$-G^8 H4′; q, H_p-T^7 H4′; r, $H_{m,m'}$-T^7 H4′; s, H_p-G^8 H5′/H5″; t, $H_{m,m'}$-G^8 H5′/H5″; u, $H_{m,m'}$-C^{18} H5′/H5″. (B) The S(12,2) adduct: a, $H_{\beta'}$-T^7 N3H; b, $H_{\beta''}$-T^7 N3H; c, $H_{\beta'}$-$^{S\text{-}SO}G^6$ N1H; d, $H_{\beta''}$-$^{S\text{-}SO}G^6$ N1H; e, $H_{\beta'}$-$^{S\text{-}SO}G^6$ 2-NH; f, $H_{\beta''}$-$^{S\text{-}SO}G^6$ 2-NH; g, H_b-T^7 N3H; h, H_b-G^5 N1H (spin diffusion); i, H_b-$^{S\text{-}SO}G^6$ N1H; j, H_b-$^{S\text{-}SO}G^6$ 2-NH; k, $H_{o,o',m,m'}$-T^7 N3H (spin diffusion); l, $H_{o,o',m,m'}$-G^5 N1H; m, $H_{o,o',m,m'}$-$^{S\text{-}SO}G^6$ N1H; n, H_p-$^{S\text{-}SO}G^6$ 2-NH (spin diffusion); o, $H_{o,o',m,m'}$-$^{S\text{-}SO}G^6$ 2-NH. (C) The S(12,2) adduct: a, H_o-T^7 CH_3 (spin diffusion); b, $H_{\beta'}$-T^7 H1′; c, $H_{\beta''}$-T^7 H1′; d, H_p-T^{19} H5′; e, H_p-T^{19} H5″; f, $H_{o,o',m,m'}$-$H_{\beta'}$ (Figure 3 B, a); g, $H_{o,o',m,m'}$-$H_{\beta''}$ (Figure 3 B, b); h, $H_{o,o',m,m'}$-T^{19} H5′; i, $H_{o,o',m,m'}$-T^{19} H5″; j, $H_{\beta'}$-A^{16} H2; k, $H_{\beta''}$-A^{16} H2; l, H_b-T^7 H1′; m, H_p-T^7 H4′; n, $H_{o,o',m,m'}$-T^7 H4′; o, $H_{o,o',m,m'}$-H_b (Figure 3 B, e); p, H_b-A^{16} H2; q, H_p-T^{19} H1′; r, H_p-C^{18} H1′; s, $H_{o,o',m,m'}$-$^{S\text{-}SO}G^6$ H1′; t, $H_{o,o',m,m'}$-T^{19} H1′; u, $H_{o,o',m,m'}$-T^7 H1′; v, $H_{o,o',m,m'}$-C^{18} H1′. NOEs involving exchangeable protons were obtained in buffer containing 9:1 H_2O:D_2O.

7.36 ppm (peak e), H_o and $H_{o'}$ were judged to be isochronous. H_m and $H_{m'}$ were assigned to the resonance of area 4 located at δ 7.36 ppm.

A total of 37 NOE cross peaks were identified between styrene oxide and DNA protons in the S(12,2) oligomer. In Figure 4B cross peaks were observed between $H_{\beta'}$ and T^7 N3H, and $^{S\text{-}SO}G^6$ N1H, and $^{S\text{-}SO}G^6$ 2-NH (peaks a, c, and e), and between $H_{\beta''}$ and T^7 N3H, $^{S\text{-}SO}G^6$ N1H, and $^{S\text{-}SO}G^6$ 2-NH (peaks b, d, and f). H_b showed cross peaks to T^7 N3H, G^5 N1H, $^{S\text{-}SO}G^6$ N1H, and $^{S\text{-}SO}G^6$ 2-NH (peaks g−j). The overlapped $H_{o,o',m,m'}$ resonances showed NOEs to T^7 N3H, G^5 N1H, $^{S\text{-}SO}G^6$ N1H, and $^{S\text{-}SO}G^6$ 2-NH (peaks k-m and o),

while H_p showed an NOE to $^{S\text{-}SO}G^6$ 2-NH (peak n). In Figure 4 C a cross peak was observed between H_o and T^7 CH_3 (peak a), which was believed to result from spin diffusion. Both $H_{\beta'}$ and $H_{\beta''}$ showed NOEs to T^7 H1′ (peaks b and c), and A^{16} H2 (peaks j and k). Of the aromatic protons, H_p showed NOEs to T^{19} H5′/H5″ (peaks d and e), T^7 H4′ (peak m; probably resulting from spin diffusion), T^{19} H1′ (peak q), and C^{18} H1′ (peak r, probably also resulting from spin diffusion). The overlapped $H_{o,o',m,m'}$ resonances showed NOEs to T^7 CH_3 (peak a), which was believed to result from spin diffusion, T^{19} H5′/H5″ (peaks h and i), T^7 H4′ (peak n), $^{S\text{-}SO}G^6$ H1′, T^{19} H1′, T^7 H1′, and C^{18} H1′ (peaks s−v). Finally, H_b showed a cross peak to A^{16} H2 (peak p). These NOEs established the 5′-orientation of the SO phenyl ring relative to $^{S\text{-}SO}G^6$.

Chemical Shift Perturbations. (a) The R(12,2) Adduct. The greatest disturbances in chemical shift for the nonexchangeable minor groove protons of the modified strand of the R(12,2) duplex relative to the unmodified *ras12* sequence were observed for T^7. Several major groove protons and imino protons near the adduct site also exhibited chemical shift perturbations. Pronounced upfield chemical shifts were observed for T^7 H1′, H2′, and H2″, with an increased shielding of 0.8 ppm observed for T^7 H1′. A downfield shift of 0.4 ppm was observed for $^{R\text{-}SO}G^6$ H1′. Smaller shift effects (0.1−0.25 ppm) were observed for C^{17} H1′, H2′, and H2″. In the major groove, T^7 H6 shifted upfield by 0.25 ppm upon SO adduction, and T^7 CH_3 shifted downfield by 0.1 ppm. T^7 N3H underwent a 0.3 ppm upfield shift, and $^{R\text{-}SO}G^6$ N1H shifted ∼0.2 ppm downfield relative to the corresponding imino proton in the unmodified duplex.

(b) The S(12,2) Adduct. Unlike the R(12,2) duplex, large perturbations were not observed for either major or minor groove protons, relative to the unmodified duplex. The observed changes primarily involved minor groove protons in the vicinity of the lesion, and the largest effects were observed in the 5′-direction from the adduct. These changes included G^5 H1′ which shifted upfield 0.35 ppm and C^{17} H1′ and H2″ which shifted downfield 0.25 and 0.20 ppm. In the major groove, $^{S\text{-}SO}G^6$ H8 experienced a downfield shift 0.2 ppm. Chemical shift perturbations of the imino protons were smaller than those observed for the R(12,2) adduct. G^5 N1H, $^{S\text{-}SO}G^6$ N1H, and T^7 N3H did not vary from their chemical shifts in the corresponding unmodified oligomer.

Structural Refinement. The rapid rotation of the styrene ring in each of the R- and S(12,2) adducts complicated the estimation of interproton distances at and next to the lesion site, since NOEs observed between the ortho and meta protons represented time-averaged values over o,o′ and m,m′ positions. The assumption was made that, in each case, the observed NOE resulted from only one (i.e., o or o′, m or m′) position. The assignment of specific NOEs to o, o′, m, or m′ was made by inspection of the IniB structure built with the SO phenyl ring oriented in the 3′-direction from $^{R\text{-}SO}G^6$ [in the case of the R(12,2) adduct] or with the SO phenyl ring oriented in the 5′-direction from $^{S\text{-}SO}G^6$ [in the case of the S(12,2) adduct]. Consequently, the styrene−DNA restraints were less defined, and larger bounds were placed on them.

Internuclear Distances. For the R(12,2) adduct, 309 experimental intensities, supplemented with calculated intensities from IniB, were used in MARDIGRAS calculations. For the S(12,2) adduct, 281 experimental intensities, supplemented with calculated intensities from IniB, were used.[4] In each case, individual distances calculated by MARDIGRAS were removed if the values were calculated to be greater than 5 Å. Poor distances, usually due to errors in intensity measurements arising from spectral overlap or from cross peaks close to the water resonance whose intensities were altered by the water presaturation pulse used during acquisition of NOESY spectra, were removed if they were inconsistent with a reasonable structure.

The final distance set for the R(12,2) adduct consisted of 251 interproton distances, listed in Table 9S of the Supporting Information. Of these, 145 were intraresidue restraints, 91 were interresidue restraints, and 15 were styrene−DNA restraints. The numbers of inter- and intranucleotide restraints at each base pair are summarized in Table 5S in the Supporting Information. An average of 25 intranucleotide, internucleotide, and empirical distances were obtained for each base pair. The final distance set for the S(12,2) adduct consisted of 226 interproton distances, listed in Table 10S of the Supporting Information. Of these, 121 were intraresidue restraints, 97 were interresidue restraints, and 8 were styrene−DNA restraints. The inter- and intranucleotide restraints at each base pair are summarized in Table 6S in the Supporting Information. In addition, 20 styrene−DNA restraints were estimated from overlapped NOEs using an IniB structure where the styrene orientation agreed with the chemical shift perturbation data. Large upper and lower boundaries were used for these restraints. Therefore, an average of 25 intranucleotide, internucleotide, and empirical distances was obtained for each base pair.

For both adducted oligodeoxynucleotides, the distribution of these distances was unequal, with some base pairs being better characterized than others. For the R(12,2) oligodeoxynucleotide, nucleotides, G^1, G^{11}, C^{12}, C^{18}, T^{19}, G^{20}, and C^{21} were under-parameterized, as measured by total experimental restraints for each base pair. G^{11}, C^{12}, C^{18}, G^{20} and C^{22} had fewer than 5 intranucleotide restraints. Fewer than 4 internucleotide restraints were available for nucleotides G^1, C^3, G^5, T^7, T^{10}, G^{11}, T^{19}, G^{20}, and C^{21}. For the S(12,2) adduct, nucleotides G^1, G^2, C^{15}, and C^{18} were under-parameterized, as measured by total restraints. G^2, C^3, G^{11}, C^{12}, C^{15}, C^{18}, G^{20}, and C^{22} had fewer than 5 intranucleotide restraints. Fewer than 4 internucleotide restraints were available for G^1, G^2, $^{S\text{-}SO}G^6$, G^9, C^{12}, C^{18}, and C^{22}. Tables 10S and 11S in the Supporting Information show the NOE-generated distances along with the upper and lower bounds assigned to them by MARDIGRAS.

Superpositions of the final structures obtained by averaging the six IniA-based and IniB-based structures, followed by PEM (⟨rMDA⟩ and ⟨rMDB⟩), are shown in stereo in Figure 5. Figure S1 in the Supporting Information shows the superposition of the six MD-generated structures for the R- and S(12,2) duplexes based on IniA and IniB. Space-filling models of the ⟨rMDA⟩ and ⟨rMDB⟩ structures of the R- and S(12,2) duplexes are shown in Figure 6.

For both the R(12,2) and S(12,2) adducts, the rms deviation between the initial structures was large [5.2 Å for R(12,2) and 5.9 Å for S(12,2)]. However, convergence to

[4] An isotropic correlation time τ_c of 5 ns was used for both sugar and base protons in all calculations. This was based on the determination of τ_c from a fluorescence anisotropy study of an 11-mer oligodeoxynucleotide adducted to BPDE.

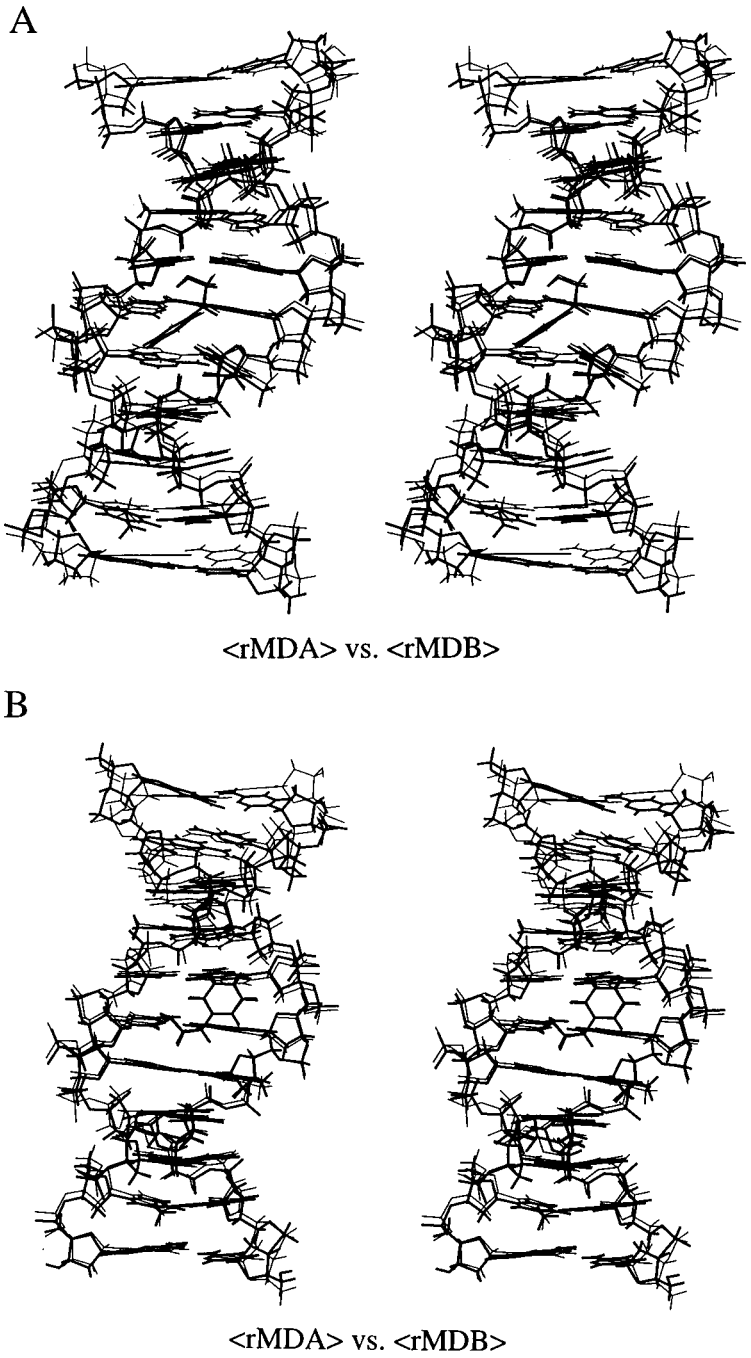

FIGURE 5: Superposition of rMDA and rMDB (bold) structures for the R(12,2) duplex (panel A) and the S(12,2) duplex (panel B).

similar structures was achieved after MD calculations. The rms deviations are summarized in Table 1 and shown graphically in Figure 2S in the Supporting Information. The final structures were B-like as revealed by the larger rms differences relative to IniA and smaller differences relative to IniB. Excluding the terminal bases, the average rms deviations between the ⟨rMDA⟩ and ⟨rMDB⟩ structures and the average refined structures were 0.95 and 0.77 Å for the R(12,2) duplex and 0.92 and 0.72 Å for the S(12,2) duplex. IniA- and IniB-based MD calculations performed in the absence of the NOE restraints did not converge, which indicated that the convergence to the final structures shown in Figure 5 was due to the NOE distance restraints.

Calculation of theoretical NOE intensities from the refined structures was performed using CORMA (Keepers & James, 1984). Table 2 shows sixth root R_1^x factors calculated for the starting structures and the MD structures for the R(12,2) and S(12,2) adducts, calculated at three NOE mixing times. Neither IniA nor IniB agreed well with the data, having $R_1^x > 10 \times 10^{-2}$. For the R(12,2) adduct, structures calculated from IniB showed improved R_1^x values relative to those calculated from IniA. For the S(12,2) adduct, at each value of NOE mixing time, structures calculated from IniA exhibited improved R_1^x values than did the set of structures calculated from IniB. However, the final structures from IniA and IniB were closer to IniB, with R_1^x values of $8.5 \pm 1.5 \times 10^{-2}$. For the R(12,2) adduct, both intra- and interresidue distances refined to approximately the same degree of accuracy, with $R_1^x = 8.5 \pm 0.5 \times 10^{-2}$. In contrast, for the S(12,2) adduct, intranucleotide distances were obtained with greater accuracy ($R_1^x = 7.2 \times 10^{-2}$ vs $9.5 \times$

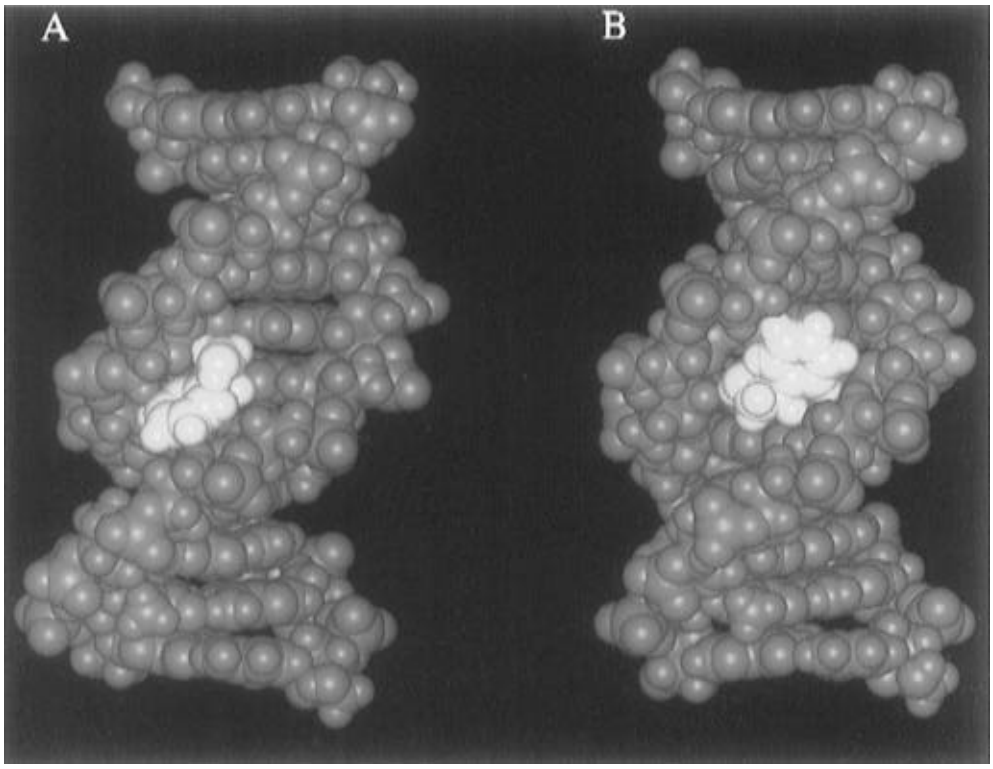

FIGURE 6: CPK representations of the final MD structures: (A) the R(12,2) duplex; (B) the S(12,2) duplex. SO is shown in yellow. These model structures are based upon averaging the coordinates from 10 MD calculations.

Table 1: Root Mean Square (rms) Deviations, Excluding the Terminal Base Pairs, between the Initial Structures, the Various rMD Structures, and the Final Average Structures of the (a) R(12,2) and (b) S(12,2) Styrene Oxide Adducts[a]

	atomic rms difference (Å)
(a) R(12,2) Styrene Oxide Adduct	
initial structures	
IniA vs IniB	5.21
rms shifts	
IniA vs ⟨rMDA⟩[a]	4.45 ± 0.24
IniB vs ⟨rMDB⟩[b]	1.60 ± 0.11
rms distributions	
⟨rMDA⟩ vs ⟨rMDA⟩	1.00 ± 0.19
⟨rMDB⟩ vs ⟨rMDB⟩	0.99 ± 0.23
⟨rMDA⟩ vs ⟨rMDB⟩	1.26 ± 0.09
⟨rMDA⟩ vs rMD[c]	0.95 ± 0.07
⟨rMDB⟩ vs rMD	0.77 ± 0.13
(b) S(12.2) Styrene Oxide Adduct	
initial structures	
IniA vs IniB	5.90
rms shifts	
IniA vs ⟨rMDA⟩[a]	4.07 ± 0.24
IniB vs ⟨rMDB⟩[b]	1.45 ± 0.16
rms distributions	
⟨rMDA⟩ vs ⟨rMDA⟩	1.14 ± 0.11
⟨rMDB⟩ vs ⟨rMDB⟩	1.02 ± 0.14
⟨rMDA⟩ vs ⟨rMDB⟩	1.13 ± 0.22
⟨rMDA⟩ vs rMD[c]	0.92 ± 0.11
⟨rMDB⟩ vs rMD	0.72 ± 0.04

[a] ⟨rMDA⟩ represents the set of six structures which emerged from MD calculations starting with IniA. [b] ⟨rMDB⟩ represents the set of six structures which emerged from MD calculations starting from IniB. [c] rMD represents the average minimized structure from all 12 MD calculations.

10^{-2}). Tables 7S and 8S in the Supporting Information list base pair-specific R_1^x values for the inner nine bases of each strand in the R(12,2) and S(12,2) duplexes. There was good agreement between the calculated structure and the data for bases away from the site of lesion, with the exception of a few bases where the cross peaks overlapped. The calculated structure became less defined at and one base 5′ and 3′ to the site of adduction, especially for the adducted strand.

DISCUSSION

The widespread utilization of styrene as a synthetic unit, the consequent risk of exposure to workers in chemical industry, and the reported genotoxicity of styrene provide impetus for structural studies of styrene oxide−DNA adducts. This work provides the first structural data for diastereomeric styrene oxide adducts at the exocyclic amino group of guanine. These structures will provide a basis for comparison with biochemical and mutagenesis data in the codon 12 sequence of the human *n-ras* protooncogene. This will allow stereospecific structure−function evaluations to be made within a coding sequence critical to oncogene activation.

Overall Structural Features. The calculations suggested that the presence of SO induced localized perturbations in the B-type helix and the patterns of base pairing and stacking at the adduct site, for the R(12,2) or S(12,2) adducts. Of the two adducts, more structural changes were observed for the R(12,2) adduct. This was consistent with the lower thermal stability of this adduct and the greater chemical shift perturbations it exhibited. At 30 °C, the $^{R\text{-}SO}G^6$ N1H and T^7 N3H resonances of the R(12,2) adduct disappeared, which suggested that these protons were in rapid exchange with solvent. The refinement data suggested out-of-plane distortions for each of these base pairs, which could be consistent with the observed weaker hydrogen bonding and increased solvent exchange.

Figure 7A,B presents a view of the stacking patterns calculated for $^{R\text{-}SO}G^6$·C^{17} and its 3′-neighbor T^7·A^{16} as compared to G^6·C^{17} and T^7·A^{16} in the unmodified *ras12* sequence, while Figure 7C shows an edgewise view from the minor groove. Structural perturbations were present, at

Table 2: Comparison of Sixth Root Residual Indices R_1^x for Starting Models and Resulting MD Structures[a−c]

	R(12,2) Adduct								
	intranucleotide R_1^x			internucleotide R_1^x			overall R_1^x		
	100 ms	200 ms	300 ms	100 ms	200 ms	300 ms	100 ms	200 ms	300 ms
IniA	19	18	17	17	16	16	18	17	16
IniB	11	11	10	11	10	10	11	11	10
rMDA	9.0	8.9	8.7	9.0	8.8	8.7	9.0	8.7	8.7
rMDB	8.8	8.7	8.7	8.5	8.4	8.3	8.6	8.6	8.4
rMD_{final}	9.0	8.7	8.7	8.6	8.3	8.3	8.8	8.4	8.6
	S(12,2) Adduct								
	intranucleotide R_1^x			internucleotide R_1^x			overall R_1^x		
	150 ms	250 ms	350 ms	150 ms	250 ms	350 ms	150 ms	250 ms	350 ms
IniA	14	14	14	17	17	17	15	15	15
IniB	7.70	7.5	7.6	11	10	10	8.8	8.7	8.7
rMDA	7.0	6.9	6.8	9.1	10	8.9	7.8	8.1	7.7
rMDB	7.5	7.3	7.3	9.5	10	9.3	8.3	8.5	8.1
rMD_{final}	7.2	7.1	7.1	9.3	10	9.1	8.1	8.3	7.9

[a] Only the inner nine base pairs were used in the calculations, to exclude end effects. [b] $R_1^x = \sum|(a_o)_i^{1/6} - (a_c)_i^{1/6}|/\sum|(a_o)_i^{1/6}|$ ($\times 10^{-2}$), where (a_o) and (a_c) are the intensities of observed (non-zero) and calculated NOE crosspeaks. [c] IniA, starting energy-minimized A-DNA; IniB, starting energy-minimized B-DNA; rMDA, average of 5 rMD structures starting from IniA; rMDB, average of five MD structures starting from IniB; rMD_{final}, average of 10 rMD structures starting from IniA and IniB.

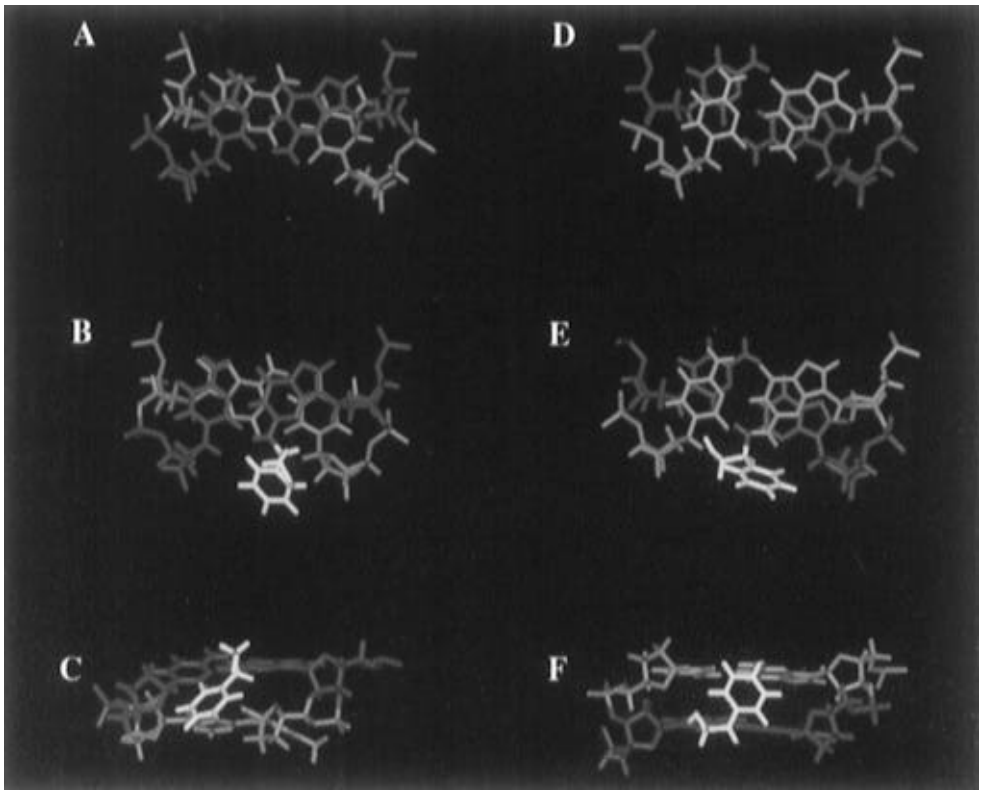

FIGURE 7: Stacking patterns of (A) G^6•C^{17} above T^7•A^{16} in the *ras12* oligodeoxynucleotide and (B) $^{R\text{-}SO}G^6$•C^{17} above T^7•A^{16} in the R(12,2) oligodeoxynucleotide. (C) Minor groove view of $^{R\text{-}SO}G^6$•C^{17} above T^7•A^{16}. Stacking patterns of (D) G^5•C^{18} above G^6•C^{17} in the *ras12* oligodeoxynucleotide and (E) G^5•C^{18} above $^{S\text{-}SO}G^6$•C^{17} in the S(12,2) oligodeoxynucleotide. (F) Minor groove view of G^5•C^{18} above $^{S\text{-}SO}G^6$•C^{17}.

and next to $^{R\text{-}SO}G^6$. Comparison of Panels A and B of Figure 7 reveals the shearing and resulting distortion of hydrogen bonding for T^7•A^{16}. Additional alterations were predicted for the stretch and propeller twist of $^{R\text{-}SO}G^6$•C^{17} and T^7•A^{16}, suggesting a weakening of these two base pairing interactions. The increased twist calculated for the $^{R\text{-}SO}G^6$→T^7 base step pushed the sugar moiety of T^7 toward the minor groove, causing T^7 H1′ and H2″ to protrude into the minor groove. Consequently, T^7 H1′ was located directly under the styrene phenyl ring, consistent with the 0.75 ppm upfield chemical shift observed for T^7 H1′ relative to the unmodified duplex. The 0.3 ppm upfield shifts of the T^7 N3H, ∼0.2 ppm downfield shift of the $^{R\text{-}SO}G^6$ N1H, and ∼1.5 ppm downfield shift of the $^{R\text{-}SO}G^6$ N2H resonances were likely due to ring current effects of the adjacent SO phenyl ring. The insertion of SO into the minor groove was calculated to increase minor groove width at and next to the lesion. This was estimated to be 1−2 Å from in the R(12,2) adduct from interstrand phosphorus-to-phosphorus distances for G^5•C^{18}, $^{R\text{-}SO}G^6$•C^{17}, and T^7•A^{16}.

Figure 7D,E presents a view of the stacking patterns calculated for $^{S\text{-}SO}G^6$•C^{17} and its 5′-neighbor G^5•C^{18} as compared to G^6•C^{17} and G^5•C^{18} in the unmodified *ras12* sequence, while Figure 7F shows an edgewise view from

the minor groove. This adduct was more readily accommodated within the minor groove, with less disturbance in chemical shift and helical parameters than the R(12,2) adduct. In the calculated structures for the S(12,2) adduct, a 9.6 Å increase in the roll of the $^{S\text{-}SO}G^6\cdot C^{17}\rightarrow G^5\cdot C^{18}$ base steps, a 0.4 Å decrease in slide of the $A^4\cdot T^{19}\rightarrow G^5\cdot C^{18}$ base step, a 0.6 Å increase in slide of the $G^5\cdot C^{18}\rightarrow {}^{S\text{-}SO}G^6\cdot C^{17}$ base step, and a 2.6 Å increase in opening of the $^{S\text{-}SO}G^6\cdot C^{17}$ base pair were detected. The 0.35 ppm upfield shift of G^5 H1′ and 0.24 and 0.20 ppm downfield shifts of C^{17} H1′ and H2″ were likely due to slight alterations in the base stacking patterns around the site of adduction. The 1.9 ppm downfield shift of $^{S\text{-}SO}G^6$ N2H was likely due to ring current shielding effects. A smaller increase of 0.6−1.3 Å in minor groove width was noted for the S(12,2) adduct.

The refined structures of the R- and S(12,2) adducts suggested that, for the right-handed DNA helix, the 3′-facing R(12,2) diastereomer should encounter greater steric hindrance than the 5′-facing S(12,2) diastereomer. This results from the relative orientations of the minor groove *R*- and *S*-stereoisomeric adducts: the *R* diastereomer clashes with the modified strand in the 3′-direction, while the *S* diastereomer is roughly parallel to the minor groove in the 5′-direction. This notion is consistent with the greater observed perturbations of the R(12,2) adduct. The structures also suggest the potential role of the 3′-neighbor base pair in modulating adduct properties for the *S*-diastereomer, and conversely, the potential role of the 5′-neighbor base pair in the properties of the *R*-diastereomer. Structural studies of the sequence isomeric R- and S(12,1) α-styrene oxide adducts designed to test this hypothesis are underway.

For the unmodified *ras12* duplex (Zegar & Stone, 1996), structural refinement revealed local variations in roll, slide, and rise helical parameters associated with the 3 R-Y-R steps, as predicted from crystallographic data (Calladine, 1982; Dickerson, 1983). Comparison of the R- and S(12,2) duplexes with the unmodified *ras12* duplex demonstrated that each exhibited increased negative roll at base step $^{R\text{-}SO}G^6\rightarrow T^7$ or $^{S\text{-}SO}G^6\rightarrow T^7$, as predicted by the Calladine rules. The S(12,2) duplex showed increased negative slide at $^{S\text{-}SO}G^6\rightarrow T^7$ but not the anticipated increased rise predicted. In contrast, the R(12,2) adduct did not exhibit predicted alterations of slide or rise at base step $^{R\text{-}SO}G^6\rightarrow T^7$. The better agreement between the S(12,2) duplex and the Calladine predictions as compared to the R(12,2) duplex correlates with the improved fit of the S(12,2) adduct within the minor groove. It will be interesting to determine whether stereospecific differences in minor groove fit of the R- and S(12,2) adducts are reflected in repair or mutagenesis.

Dynamics of the Styrene Ring. The styrene ring rotated rapidly on the NMR time scale at 30 °C.[5] The $H_{o,o'}$ and $H_{m,m'}$ styrene ring protons were equivalent, analogous to rapid ring flips of phenylalanine and tyrosine resonances within proteins (Wuthrich & Wagner, 1978). This contrasted with two major groove (*R*)-α-(*N*^{6}-adenyl)styrene oxide adducts, which displayed slow rotation of the styrene phenyl ring (Feng et al., 1995). No evidence was observed for rotation of the adduct about the guanyl N^2-C_α bond that would interchange the orientation of the styrene ring within the major groove among the 3′- and 5′-directions.

Potential for Formation of a Hydrogen Bond between the SO Hydroxyl Group and DNA. The nonequivalence of the SO methylene protons suggested the potential for hydrogen bond formation between the hydroxyl group and DNA. Inspection of the R(12,2) refined structures suggested that hydrogen bonding could occur between C^{18} O2 or O4′ and the hydroxyl. MD calculations confirmed the potential for a hydrogen-bonding interaction between the styrene hydroxyl group and C^{18} O4′. Likewise, for the S(12,2) adduct, the refinement suggested hydrogen bonding could occur between C^{17} O2 and the hydroxyl group. However, in both instances, no evidence for such interactions was observed, possibly due to rapid exchange with solvent.

Comparison with PAH−Guanine Adducts. The R- and S(12,2) SO adducts can be compared to *anti-trans*-benzo[*a*]pyrene (Cosman et al., 1992, 1994a,b; De Los Santos et al., 1992; Fountain & Krugh, 1995) and 5-methylchrysene (Cosman et al., 1995b) adducts at guanine N2. PAH adducts were classified into two fundamentally different conformations: type I adducts were intercalated, while type II were groove binders (Geacintov et al., 1982). The R- and S(12,2) SO adducts were of type II. The 10(*R*)- and 10(*S*)-*anti-trans*-benzo[*a*]pyrene adducts, in which the pyrene moieties were of equivalent stereochemistries to the R- and S-SO adducts discussed in the present work, also exhibited type II conformation (Cosman et al., 1992; De Los Santos et al., 1992; Fountain & Krugh, 1995). As for the type II (+)-10(*R*)-*anti-trans*-B[*a*]P adduct, the R(12,2) SO adduct was situated edgewise in the minor groove with the aromatic moiety oriented toward the 3′-end of the modified strand. Like the corresponding (−)-10(*S*)-*anti-trans*-B[*a*]P adduct, the styrene moiety of the S(12,2) isomer was in the minor groove with the styrene ring toward the 5′-direction.

One difference between the S(12,2) α-styrene oxide adduct and the 10(*S*)-*anti-trans*-B[*a*]P adduct was the orientation of the aromatic moiety. The PAH ring system was oriented edgewise in the groove, while for the styrene adduct, the calculations suggested a flat orientation of the styrene ring. This difference could reflect the *ras* codon 12 sequence context: for the S(12,2) adduct the 5′-neighbor to $^{S\text{-}SO}G^6$ was guanine. Studies of 3′-oriented B[*a*]P adducts in a guanine repeat sequence suggested that 5′-neighbor guanine 2-amino groups promoted bending (Mao et al., 1995; Xu et al., 1995). Structural refinement of the S(12,2) adduct did not predict bending. This may be a consequence of facile rotation of the styrene moiety, allowing it to assume the flat orientation in the minor groove, a position which is not feasible for the bulkier PAH adduct.

Biological Implications. The R(12,2) and S(12,2) adducts examined in this work provide model systems for the stereochemical consequences of SO adduction at guanine N2, within a DNA sequence in which mutagenesis is expected to activate the *n-ras* protooncogene. The hypothesis that reactive chemical species modify genomic DNA in somatic cells, leading to adduct-induced mutagenesis (Miller, 1970, 1978), is prevalent. The significance of the R(12,2) and S(12,2) SO adducts with regard to human carcinogenesis remains to be established. Concerns regarding styrene toxicity are due to the wide utilization of styrene in the

[5] The question arose as to whether the $H_{o,o'}$ and $H_{m,m'}$ styrene protons were equivalent due to rapid rotation of the aromatic ring or whether they were nonequivalent but not resolvable in the 500 MHz spectrum. A $^{13}C-^{1}H$ correlated spectrum showed that the styrene carbon resonances were also clustered and revealed three cross peaks between the styrene phenyl protons (7.29−7.36 ppm) and in the normal phenyl ^{13}C region (127−128 ppm).

chemical manufacturing industry, and its reported mutagenicity in various cell lines, including those from humans (Ott et al., 1980; Hodgson & Jones, 1985; Matanoski & Schwarts, 1987; Wong, 1990). SO adducts can be detected and examined *in vitro*, but the adduct spectrum in human cells has not been characterized.

Support for the hypothesis that chemical carcinogens induce mutations in codon 12, and thereby activate *ras*, is circumstantial. It comes from comparison of the types of mutations found in tumors which developed subsequent to carcinogen exposure, to the known or suspected chemical reactivity of the specific carcinogens. The polycyclic aromatic hydrocarbon benzo[*a*]pyrene was implicated as a causal factor in point mutations at codon 12 (Marshall et al., 1984; Vousden et al., 1986; Quintanilla et al., 1986; Bizub et al., 1986), as was *N*-nitroso-*N*-methylurea (Zarbl et al., 1985). The nitrosomethylurea evidence remains particularly controversial. More recent data revealed that rat *h-ras* mutants in codon 12 arose spontaneously during pubertal growth of the mammary gland and were not induced by nitrosomethylurea (Cha et al., 1994). The latter report illustrated the need to demonstrate a direct linkage between adduction in the codon 12 sequence and subsequent mutagenesis. Nevertheless, it continues to seem likely that electrophilic species can form adducts in the codon 12 sequence, which provide one potential avenue toward the induction of activating mutations.

One factor which may contribute toward determining the fate of potential SO guanine N2 adducts, is the ability of replication complexes to bypass the damage site (Latham et al., 1993, 1995; Latham & Lloyd, 1994). The R(12,2) and S(12,2) oligodeoxynucleotides were examined using several bacterial and eukaryotic polymerases in an *in vitro* replication system. Primer extension studies using HIV-1 reverse transcriptase, Klenow fragment (exo^- and exo^+), Sequenase 2.0, T4 holoenzyme, and human polymerases α and β revealed the R(12,2) and S(12,2) adducts blocked trans-lesion polymerization opposite and one base 3′ to the lesion.[6] This contrasted with primer extension reactions catalyzed by the exo^- Klenow using oligodeoxynucleotides with four stereoisomers of B[*a*]P adducted to N2 of guanine, in the 5′-d(CXC)-3′ sequence, which either caused G→T transversions or 1−3 base deletions. Studies using exo^+ Klenow revealed that all isomers of B[*a*]P blocked replication opposite and one base before the lesion (Shibutani et al., 1993). It is possible that the observation of replication blockage with exo^- Klenow induced by the R- and S(12,2) adducts, but not the benzo[*a*]pyrene adducts, was the result of the different 5′-d(GXT)-3′ sequence of the *ras12* oligodeoxynucleotide. In the B[*a*]P replication studies, the influence of the base 5′ to the lesion was noted (Shibutani et al., 1993). Conformational equilibration specific to the benzo[*a*]pyrene adducts could also play a role (Rodriguez & Loechler, 1993a). Experiments designed to test the fate of the R(12,2) and S(12,2) SO adducts *in vivo* are in progress.

Summary. Two diastereomeric (*R*)- and (*S*)-α-(N^2-guanyl)styrene oxide adducts at the (12,2) locus in the *ras12* protooncogene coding sequence were accommodated within the minor groove of DNA. The orientation of the styrenyl moiety was dictated by the stereochemistry at the benzylic carbon, with the R(12,2) diastereomer facing in the 3′-direction and oriented edgewise in the minor groove, while the S(12,2) diastereomer faced the 5′-direction from the site of adduction and was oriented flat in the minor groove. The R(12,2) adduct created greater structural perturbation, probably due to steric clashes with the 3′-neighbor base pair.

[6] Gary J. Latham and R. Stephen Lloyd, personal communication.

ACKNOWLEDGMENT

We thank Mr. Jason P. Weisenseel for assistance with structural refinement. Mr. Markus Voehler assisted with NMR spectroscopy. Mr. Gary J. Latham and Professor R. Stephen Lloyd (The University of Texas Medical Branch, Galveston) provided helpful discussions. Ms. Rebecca Tinkham assisted with the preparation of the manuscript.

SUPPORTING INFORMATION AVAILABLE

Tables 1S−10S, which detail the ^{1}H NMR chemical shift assignments, the distributions of NOE restraints, and the experimental distances and classes of restraints for the R(12,2) and S(12,2) adducted oligodeoxynucleotides, Figure 1S showing the superposition of the final structures obtained by averaging the six IniA-based and IniB-based structures, followed by PEM (⟨rMDA⟩ and ⟨rMDB⟩), and Figure 2S showing rms deviations for the structures emergent from the IniA- and IniB-based calculations (27 pages). Ordering information is given on any current masthead page.

REFERENCES

Arnott, S., & Hukins, D. W. L. (1972) *Biochem. Biophys. Res. Commun. 47*, 1504−1509.
Barbacid, M. (1987) *Annu. Rev. Biochem. 56*, 779−827.
Bax, A., & Davis, D. G. (1985) *J. Magn. Reson. 65*, 355−360.
Bax, A., Sklenar, V., & Clore, G. M. (1987) *J. Am. Chem. Soc. 109*, 6511−6513.
Benasutti, M., Ejadi, S., Whitlow, M. D., & Loechler, E. L. (1988) *Biochemistry 27*, 472−481.
Bizub, D., Wood, A. W., & Skalka, A. M. (1986) *Proc. Natl. Acad. Sci. U.S.A. 83*, 6048−6052.
Bodenhausen, G., Kogler, H., & Ernst, R. R. (1984) *J. Magn. Reson. 58*, 370−388.
Boelens, R., Scheek, R. M., Dijkstra, K., & Kaptein, R. (1985) *J. Magn. Reson. 62*, 378−386.
Boles, T. C., & Hogan, M. E. (1984) *Proc. Natl. Acad. Sci. U.S.A. 81*, 5623−5627.
Boles, T. C., & Hogan, M. E. (1986) *Biochemistry 25*, 3039−3043.
Bonatti, S., Abbondandolo, A., Corti, G., Fiorio, R., & Mazzaccaro, A. (1978) *Mutat. Res. 52*, 295−300.
Borer, P. N. (1975) in *Handbook of biochemistry and molecular biology*, CRC Press, Cleveland, OH.
Borgias, B. A., & James, T. L. (1990) *J. Magn. Reson. 87*, 475−487.
Brooks, B. R., Bruccoleri, R. E., Olafson, B. D., States, D. J., Swaminathan, S., & Karplus, M. (1983) *J. Comput. Chem. 4*, 187−217.
Brunger, A. T. (1992) in *X-Plor. Version 3.1. A system for X-ray Crystallography and NMR*, Yale University Press, New Haven, CT.
Calladine, C. R. (1982) *J. Mol. Biol. 161*, 343−352.
Cha, R. S., Thilly, W. G., & Zarbl, H. (1994) *Proc. Natl. Acad. Sci. U.S.A. 91*, 3749−3753.
Chary, P., Latham, G. J., Robberson, D. L., Kim, S. J., Han, S., Harris, C. M., Harris, T. M., & Lloyd, R. S. (1995) *J. Biol. Chem. 270*, 4990−5000.
Cheh, A. M., Yagi, H., & Jerina, D. M. (1994) *Biochemistry 33*, 12911−12919.
Christner, D. F., Lakshman, M. K., Sayer, J. M., Jerina, D. M., & Dipple, A. (1994) *Biochemistry 33*, 14297−14305.
Clore, G. M., Gronenborn, A. M., Carlson, G., & Meyer, E. F. (1986) *J. Mol. Biol. 190*, 259−267.

Cooper, G. M. (1982) *Science 218*, 801−806.
Cosman, M., De Los Santos, C., Fiala, R., Hingerty, B. E., Singh, S. B., Ibanez, V., Margulis, L. A., Live, D., Geacintov, N. E., Broyde, S., & Patel, D. J. (1992) *Proc. Natl. Acad. Sci. U.S.A. 89*, 1914−1918.
Cosman, M., Fiala, R., Hingerty, B. E., Laryea, A., Lee, H., Harvey, R. G., Amin, S., Geacintov, N. E., Broyde, S., & Patel, D. (1993) *Biochemistry 32*, 2488−2497.
Cosman, M., Fiala, R., Hingerty, B. E., Amin, S., Geacintov, N. E., Broyde, S., & Patel, D. J. (1994a) *Biochemistry 33*, 11507−11517.
Cosman, M., Fiala, R., Hingerty, B. E., Amin, S., Geacintov, N. E., Broyde, S., & Patel, D. J. (1994b) *Biochemistry 33*, 11518−11527.
Cosman, M., Laryea, A., Fiala, R., Hingerty, B. E., Amin, S., Geacintov, N. E., Broyde, S., & Patel, D. J. (1995a) *Biochemistry 34*, 1295−1307.
Cosman, M., Xu, R., Hingerty, B. E., Amin, S., Harvey, R. G., Geacintov, N. E., Broyde, S., & Patel, D. J. (1995b) *Biochemistry 34*, 6247−6260.
De Los Santos, C., Cosman, M., Hingerty, B. E., Ibanez, V., Margulis, L. A., Geacintov, N. E., Broyde, S., & Patel, D. J. (1992) *Biochemistry 31*, 5245−5252.
de Meester, C., Poncelet, F., Roberfroid, M., Rondelet, J., & Mercier, M. (1977) *Mutat. Res. 56*, 147−152.
DeCorte, B. L., Tsarouhtsis, D., Kuchimanchi, S., Cooper, M. D., Harris, C. M., & Harris, T. M. (1996) *Chem. Res. Toxicol.* (in press).
Dickerson, R. E. (1983) *J. Mol. Biol. 166*, 419−441.
Dittrich, K. A., & Krugh, T. R. (1991a) *Chem. Res. Toxicol. 4*, 277−281.
Dittrich, K. A., & Krugh, T. R. (1991b) *Chem. Res. Toxicol. 4*, 270−276.
Elovaara, E., Engstrom, K., Nakajima, T., Park, S. S., Gelboin, H. V., & Vainio, H. (1991) *Xenobiotica 21*, 651−661.
Feigon, J., Leupin, W., Denny, W. A., & Kearns, D. R. (1983) *Biochemistry 22*, 5943−5951.
Feng, B., Zhou, L., Passarelli, M., Harris, C. M., Harris, T. M., & Stone, M. P. (1995) *Biochemistry 34*, 14021−14036.
Fountain, M. A., & Krugh, T. R. (1995) *Biochemistry 34*, 3152−3161.
Foureman, G. L., Harris, C., Guengerich, F. P., & Bend, J. R. (1989) *J. Pharmacol. Exp. Theor. 248*, 492−497.
Geacintov, N. E., Gagliano, A. G., Ibanez, V., & Harvey, R. G. (1982) *Carcinogenesis 3*, 247−253.
Gentil, A., Margot, A., & Sarasin, A. (1986) *Proc. Natl. Acad. Sci. U.S.A. 83*, 9556−9560.
Guengerich, F. P. (1992) *FASEB J. 6*, 745−748.
Guengerich, F. P., Kim, D.-H., & Iwasaki, M. (1991) *Chem. Res. Toxicol. 4*, 168−179.
Gupta, G., Garcia, A. E., & Hiriyanna, K. T. (1993) *Biochemistry 32*, 948−960.
Hare, D. R., Wemmer, D. E., Chou, S. H., Drobny, G., & Reid, B. R. (1983) *J. Mol. Biol. 171*, 319−336.
Harris, C., Philpot, R. M., Hernandez, O., & Bend, J. R. (1986) *J. Pharmacol. Exp. Ther. 236*, 144−149.
Harris, C. M., Zhou, L., Strand, E. A., & Harris, T. M. (1991) *J. Am. Chem. Soc. 113*, 4328−4329.
Harris, T. M., Harris, C. M., Kim, S. J., Kim, H. Y., & Zhou, L. (1994) in *Polycyclic Aromatic Compounds* (Cavalieri, E., & Rogan, E., Eds.) pp 9−16, Harwood Academic Press, Philadelphia, PA.
Havel, T. F., & Wuthrich, K. (1985) *J. Mol. Biol. 182*, 281−294.
Hodgson, J. T., & Jones, P. D. (1985) *J. Work Environ. 11*, 347−352.
Hoffmann, G. R., & Fuchs, R. P. P. (1990) *J. Mol. Biol. 213*, 239−246.
Keepers, J. W., & James, T. L. (1984) *J. Magn. Reson. 57*, 404−426.
Koffel-Schwartz, N., Verdier, J. M., Bichara, M., Freund, A. M., Daune, M. P., & Fuchs, R. P. P. (1984) *J. Mol. Biol. 177*, 33−51.
Kootstra, A., Lew, L. K., Nairn, R. S., & MacLeod, M. C. (1989) *Mol. Carcinog. 1*, 239−244.
Krontiris, T. G., & Cooper, G. M. (1981) *Proc. Natl. Acad. Sci. U.S.A. 78*, 1181−1184.
Lambert, I. B., Gordon, A. J., Glickman, B. W., & McCalla, D. R. (1992a) *Genetics 132*, 911−927.
Lambert, I. B., Napolitano, R. L., & Fuchs, R. P. P. (1992b) *Proc. Natl. Acad. Sci. U.S.A. 89*, 1310−1314.
Land, H., Parada, L. F., & Weinberg, R. A. (1983) *Science 222*, 771−778.
Latham, G. J., & Lloyd, R. S. (1994) *J. Biol. Chem. 269*, 28527−28530.
Latham, G. J., Zhou, L., Harris, C. M., Harris, T. M., & Lloyd, R. S. (1993) *J. Biol. Chem. 268*, 23427−23434.
Latham, G. J., Harris, C. M., Harris, T. M., & Lloyd, R. S. (1995) *Chem. Res. Toxicol. 8*, 422−430.
Levy, D. D., Groopman, J. D., Lim, S. E., Seidman, M. M., & Kraemer, K. H. (1992) *Cancer Res. 52*, 5668−5673.
Madrid, M., Llinas, E., & Llinas, M. (1991) *J. Magn. Reson. 93*, 329−346.
Mao, B., Xu, J., Li, B., Margulis, L. A., Smirnov, S., Ya, N. Q., Courtney, S. H., & Geacintov, N. E. (1995) *Carcinogenesis 16*, 357−365.
Margulis, L. A., Ibanez, V., & Geacintov, N. E. (1993) *Chem. Res. Toxicol. 6*, 59−63.
Marien, K., Moyer, R., Lovelan, P., Van Holde, K., & Bailey, G. (1987) *J. Biol. Chem. 262*, 7455−7462.
Marien, K., Mathews, K., Van Holde, K., & Bailey, G. (1989) *J. Biol. Chem. 264*, 13226−13232.
Marion, D., Ikura, M., & Bax, A. (1989) *J. Magn. Reson. 84*, 425−430.
Marshall, C. J., Vousden, K. H., & Phillips, D. H. (1984) *Nature 310*, 586−589.
Matanoski, G. M., & Schwarts, L. (1987) *J. Occup. Med. 29*, 675−680.
Miller, E. C. (1978) *Cancer Res. 38*, 1479−1496.
Miller, J. A. (1970) *Cancer Res. 30*, 559−576.
Moyer, R., Marien, K., Van Holde, K., & Bailey, G. (1989) *J. Biol. Chem. 264*, 12226−12231.
Muench, K. F., Misra, R. P., & Humayun, M. Z. (1983) *Proc. Natl. Acad. Sci. U.S.A. 80*, 6−10.
Nakajima, T., Elovaara, E., Gonzalez, F. J., Gelboin, H. V., Raunio, H., Pelkonen, O., Vainio, H., & Aoyama, T. (1994a) *Chem. Res. Toxicol. 7*, 891−896.
Nakajima, T., Wang, R.-S., Elovaara, E., Gonzalez, F. J., Gelboin, H. V., Vainio, H., & Aoyama, T. (1994b) *Biochem. Pharmacol. 48*, 637−642.
Nelson, D. R., Kamataki, T., Waxman, D. J., Guengerich, F. P., Estabrook, R. W., Feyereisen, R., Gonzalez, F. J., Coon, M. J., Gunsalus, I. C., Goto, O., Okuda, K., & Nebert, D. W. (1993) *DNA Cell Biol. 10*, 1−51.
Nilsson, L., Clore, G. M., Gronenborn, A. M., Brunger, A. T., & Karplus, M. (1986) *J. Mol. Biol. 188*, 455−475.
Norppa, H., Sorsa, M., Pfaffli, P., & Vainio, H. (1980) *Carcinogenesis 1*, 357−361.
Norppa, H., Hemminki, K., Sorsa, M., & Vainio, H. (1981) *Mutat. Res. 91*, 243−250.
Osborne, M. R. (1990) *Chem.-Biol. Interactions 75*, 131−140.
Ott, M. G., Kolesar, R. C., Schamweber, H. C., Schneider, E. J., & Venable, J. R. (1980) *J. Occup. Med. 22*, 445−460.
Perucho, M., Goldfarb, M., Shimizu, K., Lama, C., Fogh, J., & Wigler, M. (1981) *Cell 27*, 467−476.
Pulciani, S., Santos, E., Lauver, A. V., Long, L. K., Robbins, K. C., & Barbacid, M. (1982) *Proc. Natl. Acad. Sci. U.S.A. 79*, 2845−2849.
Quintanilla, M., Brown, K., Ramsden, M., & Balmain, A. (1986) *Nature 322*, 78−80.
Ravishankar, G., Swaminathan, S., Beveridge, D. L., Lavery, R., & Sklenar, H. (1989) *J. Biomol. Struct. Dyn. 6*, 669−699.
Refolo, L. M., Conley, M. P., Sambamurti, K., Jacobsen, J. S., & Humayun, M. Z. (1985) *Proc. Natl. Acad. Sci. U.S.A. 82*, 3096−3100.
Rodriguez, H., & Loechler, E. L. (1993a) *Biochemistry 32*, 1759−1769.
Rodriguez, H., & Loechler, E. L. (1993b) *Carcinogenesis 14*, 373−383.
Ryckaert, J.-P., Ciccotti, G., & Berendsen, H. J. C. (1977) *J. Comput. Phys. 23*, 327−341.
Savela, K., & Hemminki, K. (1986) *Arch. Toxicol., Suppl. 9*, 281−285.

Schurter, E. J., Sayer, J. M., Oh-hara, T., Yeh, H. J. C., Yagi, H., Luxon, B. A., Jerina, D. M., & Gorenstein, D. G. (1995a) *Biochemistry 34*, 9009−9020.

Schurter, E. J., Yeh, H. J. C., Sayer, J. M., Lakshman, M. K., Yagi, H., Jerina, D. M., & Gorenstein, D. G. (1995b) *Biochemistry 34*, 1364−1375.

Shibutani, S., Margulis, L. A., Geacintov, N. E., & Grollman, A. P. (1993) *Biochemistry 32*, 7531−7541.

Shih, C., Padhy, L. C., Murray, M., & Weinberg, R. A. (1981) *Nature 290*, 261−264.

Sklenar, V., Brooks, B. R., Zon, G., & Bax, A. (1987) *FEBS Lett. 216*, 249−252.

Topal, M. D. (1988) *Carcinogenesis 9*, 691−696.

Topal, M. D., Eadie, J. S., & Conrad, M. (1986) *J. Biol. Chem. 261*, 9879−9885.

Voigt, J. M., & Topal, M. D. (1990) *Biochemistry 29*, 5012−5018.

Voigt, J. M., Van Houten, B., Sancar, A., & Topal, M. D. (1989) *J. Biol. Chem. 264*, 5172−5176.

Vousden, K. H., Bos, J. L., Marshall, C. J., & Phillips, D. H. (1986) *Proc. Natl. Acad. Sci. U.S.A. 83*, 1222−1226.

Wade, D. R., Airy, S. C., & Sinsheimer, J. E. (1978) *Mutat. Res. 58*, 217−223.

Warpehoski, M. A., & Hurley, L. H. (1988) *Chem. Res. Toxicol. 1*, 315−333.

Wei, S. J., Chang, R. L., Hennig, E., Cui, X. X., Merkler, K. A., Wong, C. Q., Yagi, H., Jerina, D. M., & Conney, A. H. (1994) *Carcinogenesis 15*, 1729−1735.

Wong, O. (1990) *J. Ind. Med. 47*, 753−762.

Wuthrich, K. (1986) *NMR of proteins and nucleic acids*, John Wiley & Sons, New York.

Wuthrich, K., & Wagner, G. (1978) *Trends Biochem. 3*, 227−230.

Xu, R., Mao, B., Xu, J., Li, B., Birke, S., Swenberg, C. E., & Geacintov, N. E. (1995) *Nucleic Acids Res. 23*, 2314−2319.

Zarbl, H., Sukumar, S., Arthuyr, A. V., Martin-Zanca, D., & Barbacid, M. (1985) *Nature 315*, 382−385.

Zegar, I. S., & Stone, M. P. (1996) *Chem. Res. Toxicol. 9*, 114−125.

BI952086S